Received: 1 June 2021 | Revised: 14 December 2021 | Accepted: 16 December 2021

DOI: 10.1111/bre.12651

Basin Research IAS EAGE WILEY

RESEARCH ARTICLE

The interactions of volcanism and clastic sedimentation in rift basins: Insights from the Palaeogene-Neogene Shaleitian uplift and surrounding sub-basins, Bohai Bay Basin, China

Hehe Chen[1,2,3,4] | **Xiaomin Zhu**[3] | **Robert L. Gawthorpe**[4] | **Lesli J. Wood**[5] | **Qianghu Liu**[6] | **Shunli Li**[7] | **Ruisheng Shi**[8] | **Huiyong Li**[9]

[1]School of Ocean Sciences, China University of Geosciences, Beijing, China

[2]Marine and Polar Research Center, China University of Geosciences, Beijing, China

[3]State Key Laboratory of Petroleum Resources and Prospecting, China University of Petroleum, Beijing, China

[4]Department of Earth Science, University of Bergen, Bergen, Norway

[5]Department of Geology and Geological Engineering, Colorado School of Mines, Golden, Colorado, USA

[6]College of Earth Resources, China University of Geosciences, Wuhan, China

[7]School of Energy Resources, China University of Geosciences, Beijing, China

[8]Production Optimization, China Oilfield Services Ltd., Tianjin, China

[9]Bohai Oil Field Research Institute, Tianjin Branch of CNOOC Ltd., Tianjin, China

Correspondence
Hehe Chen, China University of Geosciences, No. 29, Xueyuan Road, Beijing 100083, China.
Email: hehechen89@gmail.com

Xiaomin Zhu, China University of Petroleum, Beijing, Changping Fuxue Road No. 18, Beijing, 102249, China.
Email: xmzhu@cup.edu.cn

Funding information
Major National Science and Technology programs in the "Thirteenth Five" plan period, Grant/Award Number: 2017ZX05001002; 111 project, Grant/Award Number: B20011

Abstract

Although volcanism is an important process in the evolution of rift basins, current tectono-sedimentary models largely neglect its impact on sediment supply, transport pathways, and depositional systems. In this paper, we integrate core, well logs, and 3D seismic data from the Palaeogene-Neogene Shaleitian (SLT) uplift and surrounding sub-basins, Bohai Bay Basin, China, to investigate the sedimentology and geomorphology of a volcanic rift basin. Results of this study show that the spatial distribution of extrusive centres was strongly controlled by basement-involved intra-basin normal faults. During the early part of the syn-rift stage, the SLT uplift supplied sediments to transverse fan deltas and braided-river deltas that fringed the adjacent syn-rift depocentres. Volcanic deposits mainly occurred as relatively thin lava flow and pyroclastic facies that partially filled fault-controlled topographic lows, reducing topographic rugosity, and enhanced breaching of basement highs between syn-rift depocentres. Integration of drainage to the syn-rift depocentres and development of through-flowing axial depositional systems was enhanced. During the later part of syn-rift and in early post-rift stages, the SLT uplift was progressively inundated, reducing sediment

supply to the fringing transverse depositional systems. In contrast, axial braided-river deltas became the main depositional systems, sourced by large hinterland drainage from the Yanshan fold-belt to the northwest. Volcanism in the late syn-rift and early post-rift occurs as thick lava flow and pyroclastic facies that infill rift topographic lows and locally blocked axial fluvial systems creating isolated lakes. Within hanging wall depocentres, volcanic topographic highs split and diverted axial fluvial and deltaic systems. Furthermore, volcanism supplied large volumes of volcanic sediment to the rift resulting in increased sedimentation rates, and the development of unstable subaerial and subaqueous slopes and deposits, increasing the occurrence of landslides. Based on the observations of this study we update tectono-sedimentary models for rift basins to include volcanism.

KEYWORDS

Bohai Bay Basin, depositional systems, landscape, rift basin, sediment supply, volcanism

1 | INTRODUCTION

Most tectono-sedimentary models for rift basins focus on the interplay of tectonics, sea-level and climate controls on syn-rift sedimentation and stratigraphy (e.g. Gawthorpe & Leeder, 2000; Leeder & Gawthorpe, 1987; Leeder et al., 1996; Ravnas & Steel, 1998). These studies largely concern non-volcanic rifts, yet igneous activity, including lava eruption and intrusive magmatism, is known to be an important aspect in the evolution of many rift basins (e.g. Ebinger & Scholz, 2012; Magee et al., 2014; Menzies et al., 2002; White & McKenzie, 1989). Previous studies on volcanic influence in rifts have examined tectonic controls on volcanism (e.g. Acocella, 2014; Ferguson et al., 2010; Wolfenden et al., 2005), the volcanic-stratigraphic records (e.g. D'Elia & Martí, 2013; Hutchison et al., 2016), and the interplay between volcanism and sedimentary systems (Ebinghaus et al., 2020; Famelli et al., 2021; Hardman et al., 2019; Hole et al., 2013; Williamson & Bell, 2012). Even though the sedimentation in rifts associated with large igneous provinces has been extensively studied (i.e. the North Atlantic; Duncan et al., 2020; Ebinghaus et al., 2014; Hardman et al., 2019; Jolley et al., 2009; Millett et al., 2021; Schofield & Jolley, 2013), due to the complexity of volcanism and magmatism in basin evolution, understanding the spatial and temporal interactions between normal faulting, volcanism, and clastic depositional systems in volcanic rift basins remains challenging.

Volcanism and dynamic topography associated mantle plumes have been proven to significantly influence the landscape and its drainage networks (e.g. D'Elia et al., 2018; Hartley et al., 2011; Magee et al., 2013; Miles & Cartwright, 2010; Muravchik et al., 2011). Sediment yields in volcanic-active areas are several orders of magnitude higher than non-volcanic areas, approaching 10^7 Mg/km^2/yr (Abdelmalak et al., 2019; Hayes et al., 2002; Millett et al., 2020; Planke et al., 2000). Large-volume volcanic eruptions can cause major reorganisation of drainage patterns by creating or destroying lake bodies, shifting watersheds, and diverting major rivers (e.g. Ebinghaus et al., 2014, 2020; Hardman et al., 2019; Manville et al., 2007). Furthermore, emplacement of subterranean intrusive bodies can cause major changes in surface topography (e.g. Hartley et al., 2011; Magee et al., 2013, 2014, 2017; Miles & Cartwright, 2010; Reynolds et al., 2018). Fieldwork allows for detailed examination of volcanic products and observations on the local spatial and stratigraphic relationships associated with rift structure and sediments. However, limited or widely separated exposures often result in a relatively

Highlights

- Well and seismic data from the Bohai Bay Basin, China provide insight into tectono-sedimentology in volcanic rifts.
- Distribution of surficial and sub-surface volcanic elements with respect to rift structure.
- Volcanism significantly modifies local rift topography and has a range of interactions with sediment routings.
- Volcanism supply large volumes of volcanic detritus, affecting the scale and stability of depositional systems.
- Updated tectono-sedimentary models for rifts that include interactions of volcanism and depositional systems.

limited or complex view of the volcanic records (e.g. Martí et al., 2018; Muravchik et al., 2011; Zanchetta et al., 2004). High-resolution seismic reflection data-based analyses, calibrated by well logs and core, can provide full 3D views of volcanic bodies and allow the relationships between volcanic elements and the surrounding stratigraphy and structure to be investigated (e.g. Magee et al., 2013, 2016; Magee et al., 2014a; Planke et al., 2017; Walker et al., 2021).

This study uses seismic geomorphological analysis, integrated with borehole data, to investigate the relationships between volcanism and clastic depositional systems during the Palaeogene rift stage in the Shaleitian sub-basin of the Bohai Bay Basin, China (Figure 1). The specific objectives of this basin-scale study are to (1) identify the various depositional systems and volcanic elements in the rift; (2) explore the role of rift volcanism on rift landscape evolution and deltaic-lacustrine depositional systems; and (3) establish a tectono-sedimentary model for volcanic rift basins focusing on the interactions of volcanism and deltaic-lacustrine systems. The results of the study develop our understanding of the influence of volcanism on the development and distribution of clastic depositional systems in rift basins and enlighten hydrocarbon explorations on volcanic-rifted margins worldwide.

2 | GEOLOGICAL SETTING AND STRATIGRAPHY

The Shaleitian (SLT) sub-basin is an NW-SE-trending Palaeogene rift basin in the Bohai Bay Basin, northeast China that is approximately 150 km long and 100 km wide (Allen et al., 1997; Hou et al., 2001; Lu & Dai, 1989; Figure 1). Extension of the region began in the Early Palaeogene and continued to the Early Neogene, with the syn-rift stage occurring in the Palaeogene, represented by the Shahejie and Dongying formations (Zhang, 2000; Zhu et al., 2015; Figures 2 and 3).

The SLT uplift is a major intra-basin horst, ca. 60 km long and 40 km wide, and is subdivided into the west-SLT (WSLT) and east-SLT (ESLT) by the N-S-striking 1-fault (Liu et al., 2017; Shi et al., 2013; Zhu et al., 2015; Figure 1). This study focuses on two sub-basins around the western side of the SLT uplift; the NNW-SSE-striking Qikou sub-basin to the west, and the E-W-striking Nanpu sub-basin to the north (Figure 1). The Xinanzhuang and Baigezhuang uplifts lie to the north of the Nanpu sub-basin and are separated from it by major south-dipping normal faults (Figure 1). To the south of the Qikou sub-basin is the fault-bounded Chengzikou uplift (Figure 1).

Previous work has subdivided the basin fill into four stages: (i) early syn-rift (older than 42.0 Ma), (ii) main syn-rift (42.0 Ma–32.8 Ma), (iii) late syn-rift (32.8 Ma–24.6 Ma), and (iv) post-rift (younger than 24.6 Ma) (Hou et al., 2001; Zhu et al., 2015; Figure 3). The early syn-rift stage is only locally developed in the Nanpu and Bozhong sub-basins (Hou et al., 2001; Zhu et al., 2015; Figure 3). The main syn-rift and late syn-rift stages are characterised as a series of fault-controlled lake depocentres rimmed by deltaic shorelines, with a transition to meandering fluvial systems in the post-rift

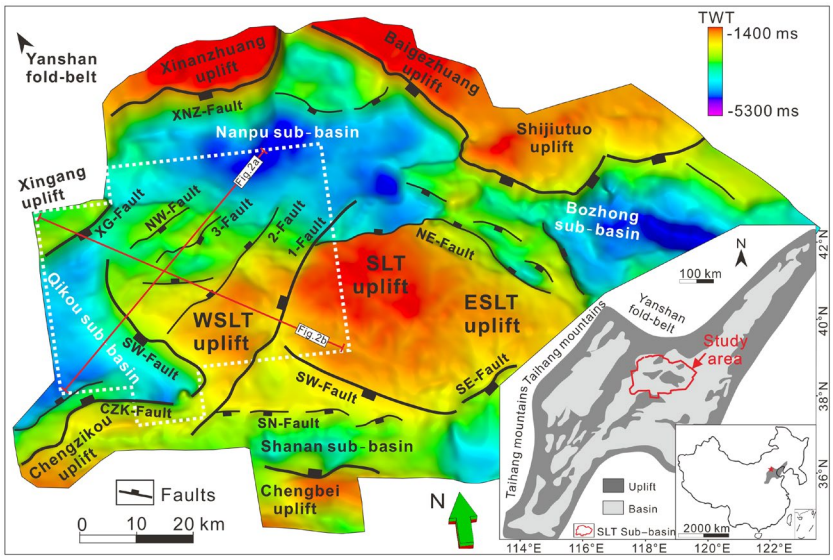

FIGURE 1 The Paleogene structural elements of the Shaleitian (SLT) Uplift and surrounding sub-basins, Bohai-Bay Basin. The base-map is an oblique view to the north of the T8 time-structure map, flattened on the T0 post-rift horizon, showing the local structural elements of the SLT Uplift and surrounding sub-basins (Modified after Liu, 2016). The inserted map shows the tectonic elements of the Bohai Bay Basin. The dotted red line marks this study area. SLT uplift, Shaleitian uplift; WSLT uplift, West Shaleitian uplift; ESLT uplift, East Shaleitian uplift

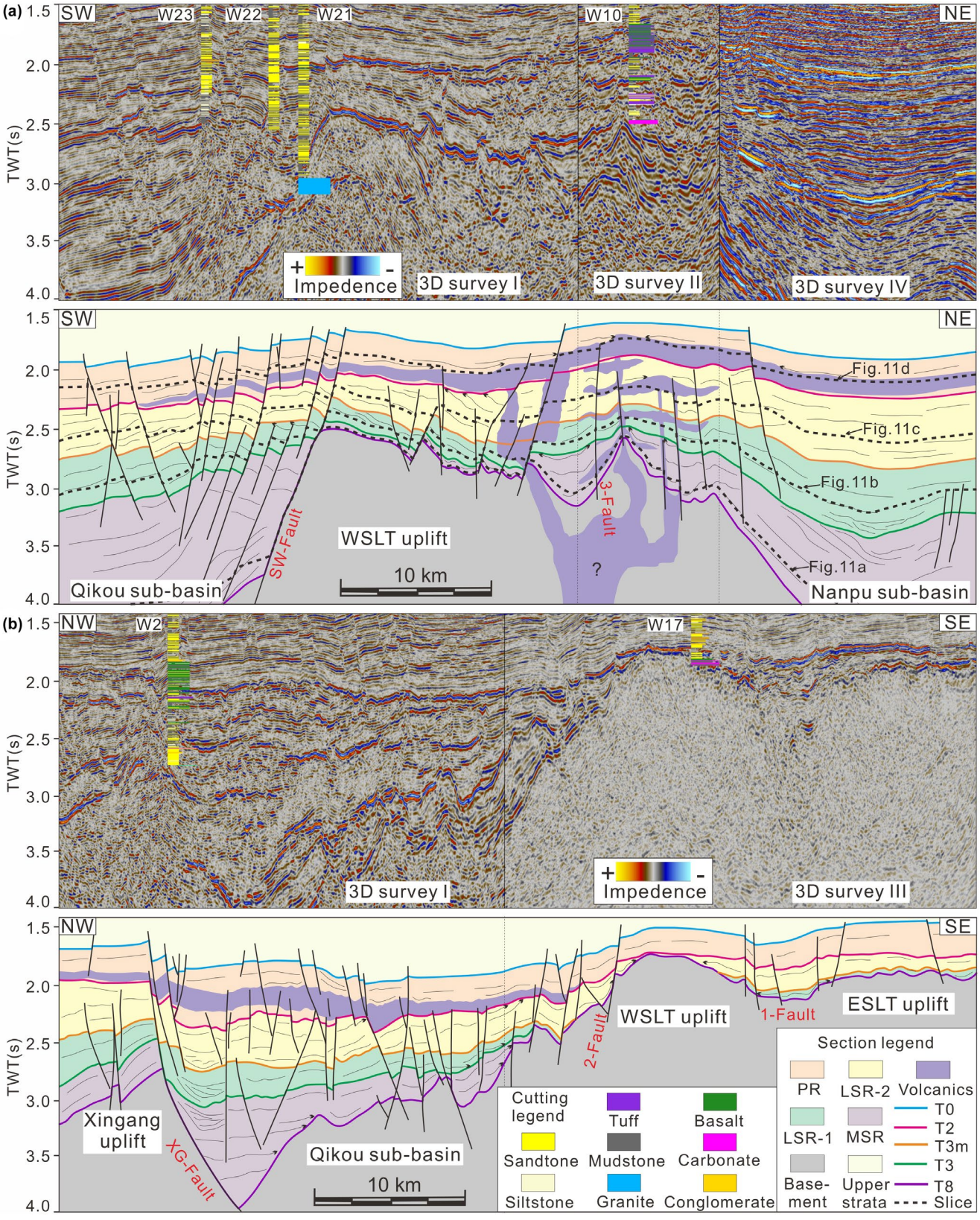

FIGURE 2 Seismic cross-sections and corresponding schematic interpretations along the rift axis and rift transverse direction of the study area. Note a few volcanic systems were identified in the main syn-rift stage and the late syn-rift stage, as the seismic resolution limits such interpretation (Schofield et al., 2017). Arrows are used to indicate truncations and onlaps. Drill cuttings and logs are used to calibrate the lithology on seismic sections. The location of these seismic sections is shown in Figure 1. PR, post-rift; LSR-1, late syn-rift stage 1; LSR-2, late syn-rift stage 2; MSR, main syn-rift

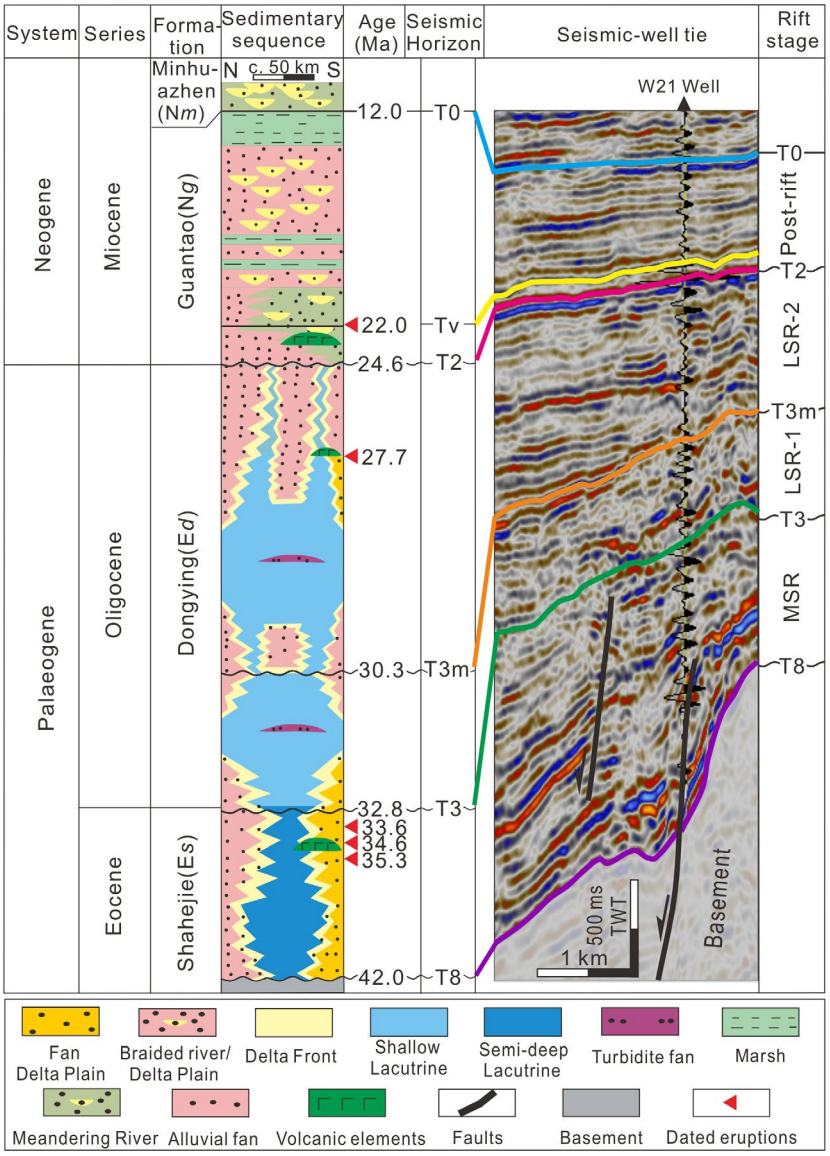

FIGURE 3 A generalized stratigraphic column of the SLT Uplift and surrounding sub-basins in the Bohai-Bay Basin (Modified after Liu, 2016). The depositional environments interpreted seismic horizons, and rift stages are shown along with the geological ages of volcanic eruptions based on zircon dating from Du et al. (2014). W21 well is tied on the seismic section for well-seismic ties. Note that the volcanic elements and depositional systems in the sedimentary sequence column are not to scale

stage (Hou et al., 2001; Liu et al., 2017; Zhu et al., 2015; Figure 3). During the main syn-rift stage, the SLT uplift, Chengzikou uplift and Xingang uplift were eroding fault-bounded highs that supplied sediment to adjacent rift basins denuded from Proterozoic and Archaean metamorphic rocks, Palaeozoic carbonates, and minor Mesozoic volcanics (e.g. Liu et al., 2017; Xu et al., 2008; Zhang, 2000; Figure 1). During the late syn-rift stage (late Oligocene), these highs were gradually submerged and buried by lacustrine sediments, and sediment to the basin was mainly sourced from outside the basin by the Yanshan fold-belt to the northwest of the study area (Liu et al., 2017; Xu et al., 2008; Zhang, 2000; Figure 1).

Volcanism in the Bohai Bay Basin produced thick successions of basalt, andesite, and trachyte interpreted to be intrusive sills and dykes and extrusive lava flows and tuffs (Liu et al., 2017; Zou et al., 2008). The interaction between volcanism and clastic depositional systems results in widespread deposition of volcanoclastic lithologies (Du et al., 2014; Xu et al., 2008; Figure 2). Within the study area, multiple phases of volcanic eruptions have been documented through zircon dating of subsurface igneous rock samples, indicating three main phases of volcanism developed during the rift evolution: (i) Late Eocene, (ii) Late Oligocene, and (iii) Early Miocene (Du et al., 2014; Xu et al., 2008; Figure 3).

3 | DATASETS AND METHODS

The dataset for this study consists of five partly overlapping 3D seismic surveys that together cover an area of about 3500 km^2 (Figure 4 and Table 1). The seismic data are presented in reverse polarity (SEG Convention), where a stratigraphic downward increase in acoustic impedance is represented by a trough (red reflection). The vertical sampling interval is 2 ms in two-way travel time

(TWT) with a record length of 6000 ms TWT (Figure 4 and Table1). Within the stratigraphic interval of interest, the dominant frequency is ca. 25 Hz and the average interval velocity of clastic strata is ca. 2000 m/s, giving a vertical resolution of ca. 20 m. As the velocity of volcanic intrusive and extrusive rocks differs significantly (e.g. Planke, 1994; Planke et al., 2005), the thickness of igneous rocks is mainly calculated from drill cuttings.

Twenty-nine exploration wells across the study area are used, each containing a suite of well logs, stratigraphic picks, and drill cuttings (Figure 4). Most of the wells penetrate the Neogene-age Guantao Formation and the Palaeogene-age Dongying Formation but terminate in the Palaeogene-age Shahejie Formation (Figure 3). Cored intervals are mostly in sandstone-rich sections. Core is used together with drill cuttings to identify lithology and to calibrate well logs, as well as support interpretation of seismic facies, and seismic geomorphology. Drill cuttings are used to identify igneous rocks and to calculate their thickness in different rift stages. The thickness of igneous and clastic rocks described in this paper all refers to the thickness as shown on drill cuttings. Thin sections of 72 sandstone samples are point counted (300 points/thin-section) and the results are used in the analysis of petrographic and sediment provenance.

Synthetic seismograms generated from sonic logs and density logs assist with tying stratigraphic horizons in key wells (W21, W7, W14, and W18) to seismic data (Figure 3). Six seismic horizons (T0, Tv, T2, T3m, T3, and T8) are mapped based on changes in seismic facies and reflector termination, or by their stratigraphic occurrence as indicated by strata documented in well data (Figure 3 and Table 2). Horizons are mapped at a general line spacing of 125 m, but mapped line spacing is closer in structurally and stratigraphically complex areas. Faults are interpreted in seismic sections with care taken to 'snap' fault-horizon cut-offs. Time-thickness maps between mapped seismic horizons are used as a proxy for subsidence to analyse the spatial and temporal variations in fault activity. The onlap terminations of the T2, T3m, T3, and T8 horizons along the SLT uplift are broadly used to define the margins of the erosional area of the uplift.

Seismic-based sedimentological and geomorphological analysis of the clastic depositional systems and volcanic elements is based on the interpretation of a combination of Root Mean Square (RMS) amplitude and variance attribute maps, calibrated by seismic facies analysis in seismic cross sections. Drill cuttings are used to calibrate RMS attribute maps and to document the presence or absence of volcanic rocks in the study area.

4 | STRUCTURAL FRAMEWORK OF THE NORTHWEST SLT UPLIFT AND SURROUNDING SUB-BASINS

The structural framework of the SLT uplift and surrounding sub-basins is best illustrated with the

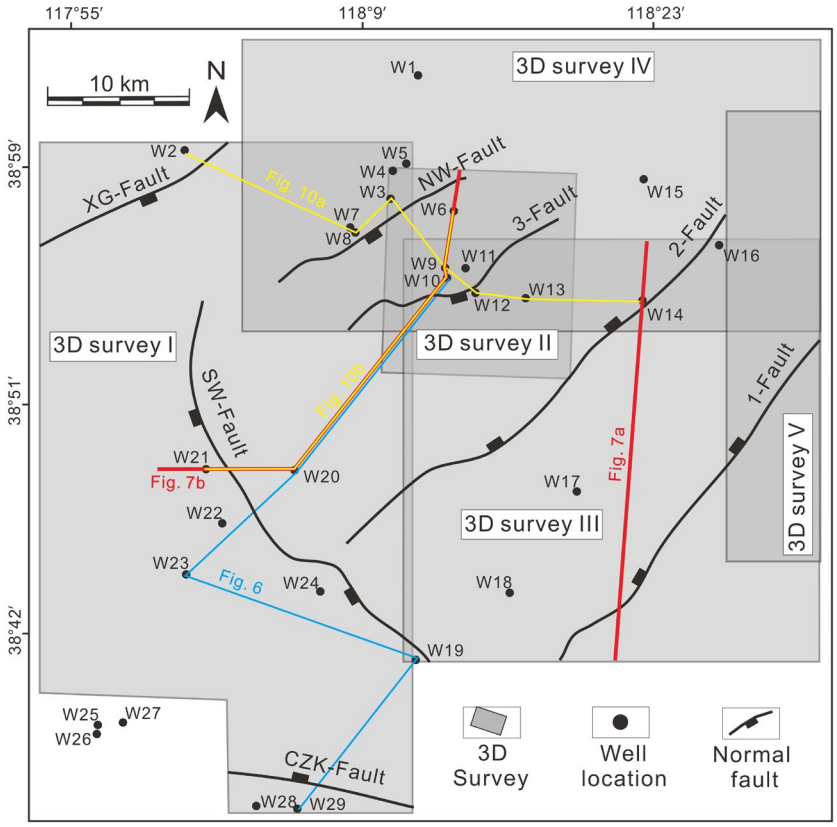

FIGURE 4 Map showing the location of 3D seismic surveys and exploration wells. The site of this map is displayed in Figure 1. The pink line indicates the position of a well-correlation panel illustrated in Figure 6. The red lines indicate the position of seismic sections in Figure 7. The blue lines indicate the position of a well-correlation panel illustrated in Figure 10. Note the seismic section in Figure 7b corresponds to the well-correlation panel in Figure 10b

TABLE 1 Summary of seismic surveys utilised in this study

Survey	Polarity	Area (km^2)	Line orientation	Line spacing (m)
3D survey I	Reverse	c. 1300	Inline = W-E	25
			Crossline = S-N	12.5
3D survey II	Reverse	c. 1000	Inline = W-E	25
			Crossline = S-N	12.5
3D survey III	Reverse	c. 200	Crossline = W-E	25
			Crossline = S-N	25
3D survey IV	Reverse	c. 800	Inline = W-E	25
			Crossline = S-N	25
3D survey V	Reverse	c. 200	Inline = W-E	25
			Crossline = S-N	25

time-structure map of the basal surface of the Shahejie Formation (T8 horizon). This surface, the base of the syn-rift, records the syn-rift deformation and shows the configurations of the main tectonic elements (Figure 1). In general, the SLT uplift is broadly E-W-striking, with a length of 80 km and a width of about 25 km (Figures 1 and 2). The geometry of the SLT uplift and adjacent half grabens is defined by the NW-SE-striking SW-Fault, and an array of NE-SW-striking faults which include a basin bounding fault, the XG-Fault, and a series of intra-rift faults; 1-Fault, 2-Fault, 3-Fault, and NW-Fault (Figures 1 and 2). The SLT uplift is subdivided by the 1-Fault into the ESLT uplift and WSLT uplift, and the study area mainly focuses on the WSLT uplift and two adjacent half-graben sub-basins; the Nanpu sub-basin and the Qikou sub-basin (Figures 1 and 2).

The Qikou sub-basin is ca. 40 km long and ca. 20 km wide (Figure 1). The deepest part of the Qikou sub-basin is in the immediate hanging wall of the CZK-Fault which has an average displacement of ca. 2400 ms TWT (ca. 2400 m) (Figures 1 and 2). The northeast boundary of the Qikou sub-basin is the 20 km long SW-Fault which has an average displacement of ca. 2000 ms TWT (ca. 2000 m) (Figures 1 and 2). The north western boundary of the Qikou sub-basin is the XG-Fault which has an average displacement of ca. 1200 ms TWT (ca. 1200 m) (Figures 1 and 2). To the north of the SLT uplift, the Nanpu sub-basin is ca. 60 km long and ca. 35 km wide (Figure 1). The north boundary of the Nanpu sub-basin is the ca. 50 km long XNZ-Fault which has an average displacement of ca. 3000 ms TWT (ca. 3000 m), with the deepest part of the Nanpu sub-basin developed in its hanging wall (Figures 1 and 2).

The NE-SW-striking intra-basin faults that dissect the WSLT uplift range in length from ca. 12 km to ca. 45 km and have average displacements of ca. 300 ms TWT (ca. 300 m) (Figure 1). They create a series of ca. 10 km wide and ca. 20 km long, NE-SW-striking tilted fault terraces that downstep the WSLT uplift to the NW (Figures 1 and 2).

5 | SEDIMENTOLOGICAL AND GEOMORPHOLOGICAL ANALYSIS OF DEPOSITIONAL SYSTEMS AND VOLCANIC ELEMENTS

5.1 | Petrographic analysis

Petrographic analysis indicates that rift interval sandstones are lithic arkoses and feldspathic litharenites with an average composition of 50.2% quartz grains, 28.6% feldspars, and 17.3% rock fragments (Figure 5a). Igneous rock fragments comprise an average of 68% of all rock fragments (Figures 5a and 6). Provenance analysis suggests the sediments were derived from recycled orogenic and dissected arc, magmatic arcs, and continental rift margin (e.g. Dickinson et al., 1983; Figure 5a,b).

The amount of igneous rock debris varies between the different rift stages (Figure 6), being slightly higher in the main syn-rift, late syn-rift stage 2, and post-rift stages compared to the late syn-rift stage 1. For example, the amount of igneous rock fragments in the late syn-rift stage 1 averages ca. 46% in well W19 and ca. 51% in well W20 compared to >60% in the other rift stages (Figure 6).

5.2 | Sedimentological and geomorphic analysis of clastic depositional systems

Based on wireline, seismic, drill cuttings, and core datasets analyses, three primary depositional systems were identified: fan deltas, braided-river deltas, and sublacustrine systems, and are described in the following section.

TABLE 2 Details of the seismic horizons mapped in this study

Name	Seismic horizon	Tectono-stratigraphic significance	Seismic reflection event	Reflection continuity	Comments
T0	Top Guantao formation	Intra post-rift	Strong trough	Very good	Flooding surface is developing apparent onlaps above it
Tv	Top Volcanic rocks	Intra post-rift	Strong peak	Good	Unconformity developing onlaps above it
T2	Top Dongying formation	Top late syn-rift	Strong trough	Good	Top unconformity of Paleogene strata and developing truncation below it
T3m	Intra Dongying formation	Intra late syn-rift	Moderate peak	Fair	Unconformity developing truncation below it
T3	Top Shahejie formation	Top main syn-rift	Weak peak	Poor	Unconformity developing onlaps above it and truncation below it
T8	Base Shahejie formation	Base main syn-rift	Moderate trough	Poor	Unconformity developing onlaps above it and truncation below it

5.2.1 | Fan deltas

Description

This depositional system is composed of large sets of medium-low amplitude clinoforms forming wedge-shaped bodies commonly located in the immediate hanging wall of basin boundary faults (Figure 7 and Table 3a). Individual clinoform foresets are up to ca. 250 ms TWT (ca. 250 m) in height with an overall oblique progradational pattern and radii that range between ca. 0.5–4 km (Figure 7 and Table 3a). Gamma-ray logs show segregated box-shaped, and bell-shaped motifs, with a calculated sand content >50%. Core through these intervals is dominated by sandstones and matrix-supported conglomerates that are composed of sub-angular to sub-rounded red granite and mud clasts (Table 3a). Some cored intervals are present as interbedded sandstones and mudstones (Table 3a).

Interpretation

The internal clinoform reflector geometry, coarse sandstone with conglomerate lithology, and location in the immediate hanging wall of normal faults suggest that these wedge-shaped bodies are fan deltas (e.g. Leeder, 2009). The locations of these fan deltas are controlled by boundary faults and they are widely developed within the main syn-rift stage and the lowermost portions of the late syn-rift stage (Figure 7 and Table 3a). The slope of the clinoform foresets ranges between ca. 15° and 25°, typical of fault-bounded Gilbert-type deltas (e.g. Corinth rift, Greece; Gawthorpe et al., 2018; Hemelsdaël et al., 2017). Based on the foreset height, water depths in the rift margin were at least ca. 250 m. Bell-shaped well-log motifs in the upper portions of these clinoform intervals are interpreted to indicate the presence of subaqueous distributary channel complexes (Table 3a). The distal parts of wedge-shaped bodies, which are calibrated by well penetrations as sandstones interbedded with mudstones are interpreted to have been deposited by turbidite and debris flows and are interpreted as fan delta-front deposits (Table 3a).

5.2.2 | Braided-river deltas

Description

This depositional system is represented on seismic data by medium-low amplitude, low-angle oblique clinoforms and shingled clinoforms, along titled hanging wall dipslopes (Figure 7 and Table 3b). The clinoforms are top-truncated, primarily composed of gently dipping foresets (ca. 4°), with individual clinoform foreset units, typically ca. 150 ms TWT (ca. 150 m) thick, and with a radius of ca. 1.5 km (Table 3b). These clinoform units prograde within the late syn-rift stage and widely developed on the fault-terraced WSLT uplift (Table 3b). Gamma-ray logs show vertically stacked,

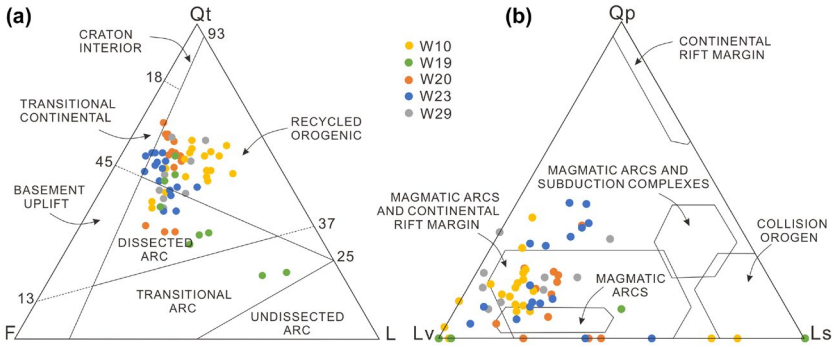

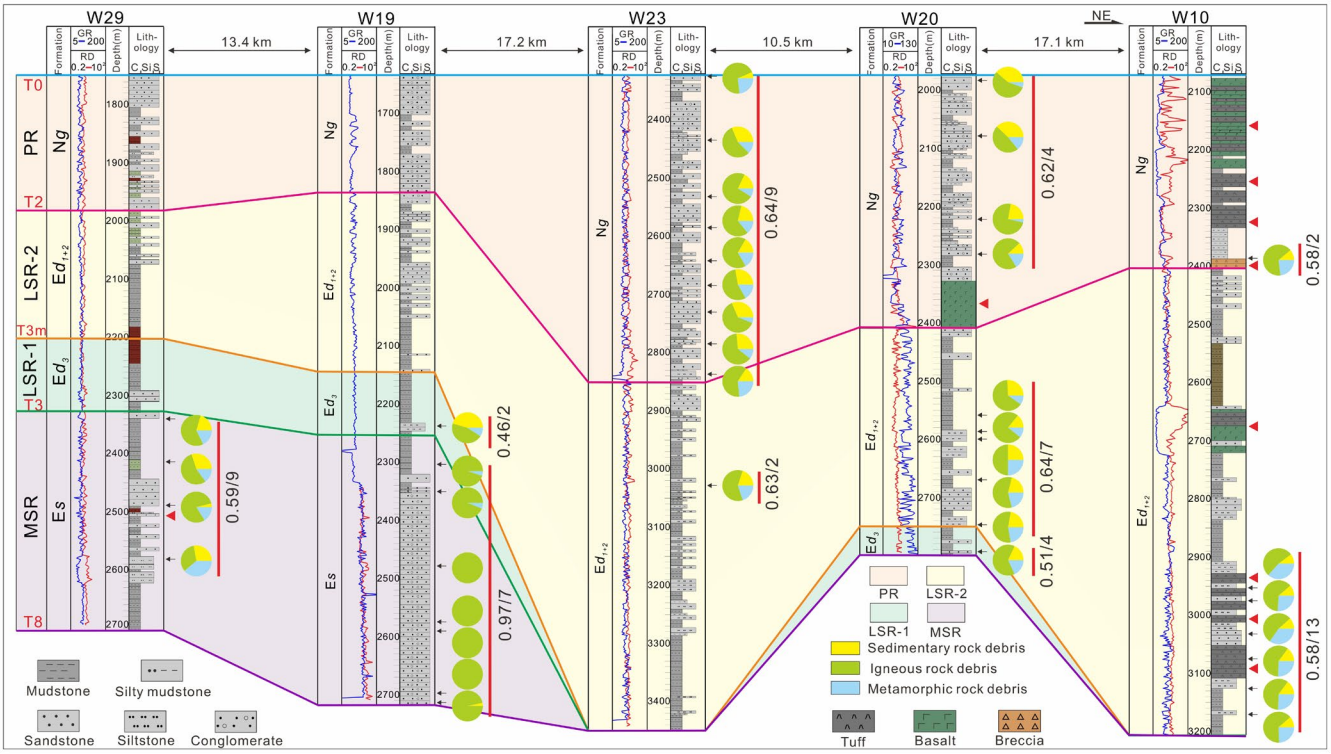

FIGURE 5 (a and b) The sediment provenance discriminating fields. Most of the sediments in this study area originated from recycled orogenic, magmatic arcs and continental rift margins. The template of the QFL plot is cited by Dickinson et al. (1983)

FIGURE 6 Well-correlation panel showing the content of different rock debris. The 0.63/2 means the average content of igneous rock fragments and sampled number. Note the content of igneous rock fragments increased during volcanism than inter-eruption stages. Abbreviations for the grain size scale: C, clay; Si, siltstone; S, sandstone

funnel- and box-shaped motifs ranging from ca. 8 m to ca. 25 m in thicknesss, and core from these intervals are composed of pebbly sandstones (ca. 10%–15% in total thickness) and grey-coloured medium- to fine-grained sandstones with an abundance of grading and cross-bedding (Table 3b). Scour surfaces widely occur at the base of graded beds (Table 3b). Core from the "toe" regions of these clinoforms comprise interbedded siltstones and mudstones (Table 3b).

Interpretation

The oblique clinoform and shingled clinoform reflector geometries indicate progradation into relatively shallow water depth (ca. <150 m). The funnel- and box-shaped well-log motifs, and widely developed scour surfaces, cross- and graded-bedding indicate the development of multi-phase distributary channels (e.g. Li et al., 2010; Table 3b), suggesting that they represent braided-river deltas (e.g. Blair & McPherson, 1994; Lunt et al., 2004). The bottomsets of the clinoform, which in core are interbedded siltstones and mudstones, are interpreted as braided-river delta-front deposits (Table 3b).

5.2.3 | Sub-lacustrine

Description

This depositional system is composed of medium- to high amplitude, parallel or weakly divergent seismic reflections, located basinward of clinoform bottomsets (Figure 7 and Table 3c). Spontaneous-potential well logs show a flat

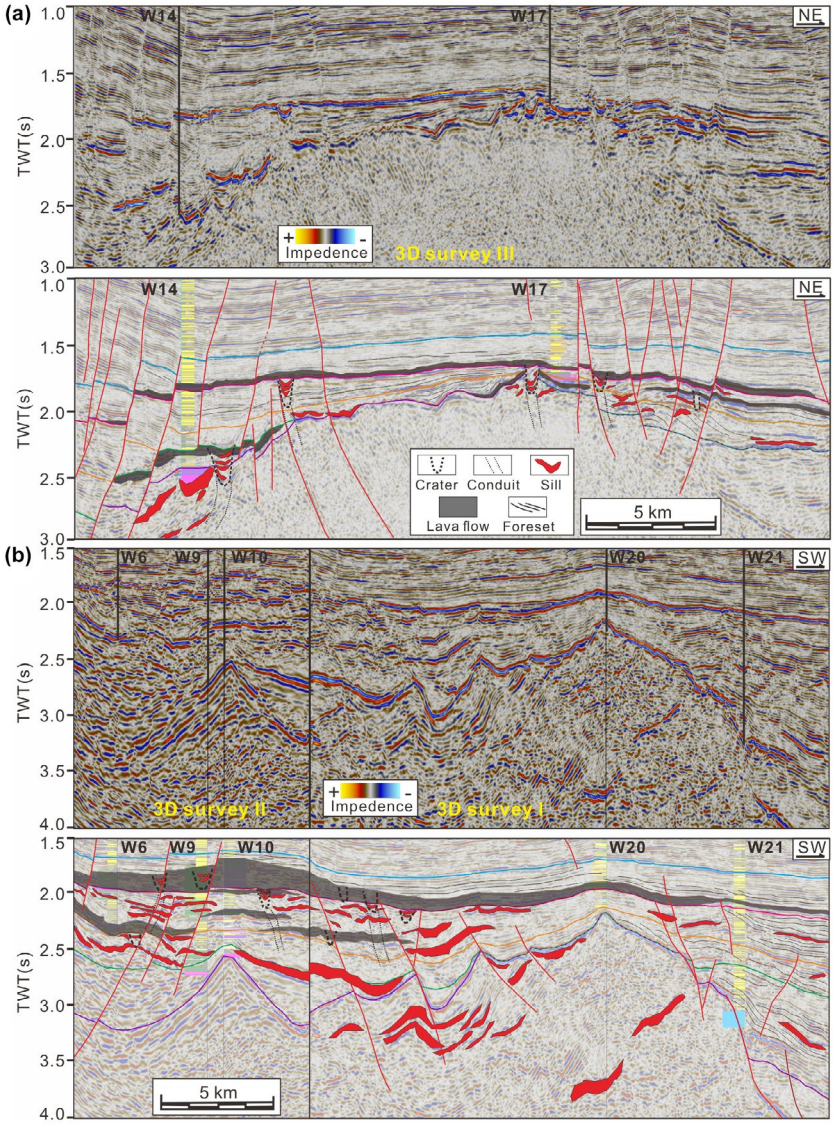

FIGURE 7 Uninterpreted and interpreted arbitrary seismic lines across the study area showing extrusive lava flows, volcanic conduit, and associated sills interplayed with clastic depositional systems. Keys for drill cuttings and horizons can find in Figure 2 and line locations are shown in Figure 4

motif and gamma-ray logs show relatively high gamma-ray values (average 95 API) and serrated motifs (Table 3c). Core intervals comprise black, thick-bedded to massive mudstones, ranging from ca. 1 to ca. 8 m, and laminated mudstones (ca. 2 m), interbedded with thin-bedded siltstones and sandstones, ranging from ca. 0.1 to ca. 1 m (Table 3c). Bioturbation is rare and where present occurs as horizontal burrows within thick-bedded mudstones (Table 3c). In addition, some low amplitude and low continuity reflection intervals, averaging ca. 100 ms TWT (ca. 100 m) thicknesses are composed of ca. 2 to ca. 5 m thick box- and funnel-shaped gamma-ray log responses within a background of high gamma mudstone (Table 3d). Cored intervals comprise matrix-supported mudclasts overlain by centimetre-scale graded fine sandstone showing Bouma Ta and Td divisions (Table 3d). This depositional system is widespread in the main syn-rift stage and late syn-rift stage 1 and gradually narrows in its distribution in the late syn-rift stage 2 and post-rift stage (Table 3d).

Interpretation

The nature of seismic reflectors in this stage and their location, basinward of deltaic clinoform bottomsets, indicate a relatively stable subaqueous environment in water depths > ca. 100 m. The high gamma-ray log response, thick-bedded to massive mudstones interbedded with siltstones suggests a low energy sub-lacustrine, basinal environment (Table 3c). The matrix-supported mudclast conglomerates and Bouma division sandstones are interpreted as debris flow and turbidite deposits, that along with their low amplitude and low continuity seismic facies, suggest the development of delta-front slumps or turbidite fans (e.g. Liu et al., 2017; Table 3d).

5.3 | Description and spatial analysis of volcanic elements

Both surficial and subsurface volcanic elements occur in the basin. Surficial elements include crater, lava flow, and

TABLE 3 Logging-core-seismic facies table of clastic depositional systems in the Shaleitian sub-basin (modified after Liu, 2016)

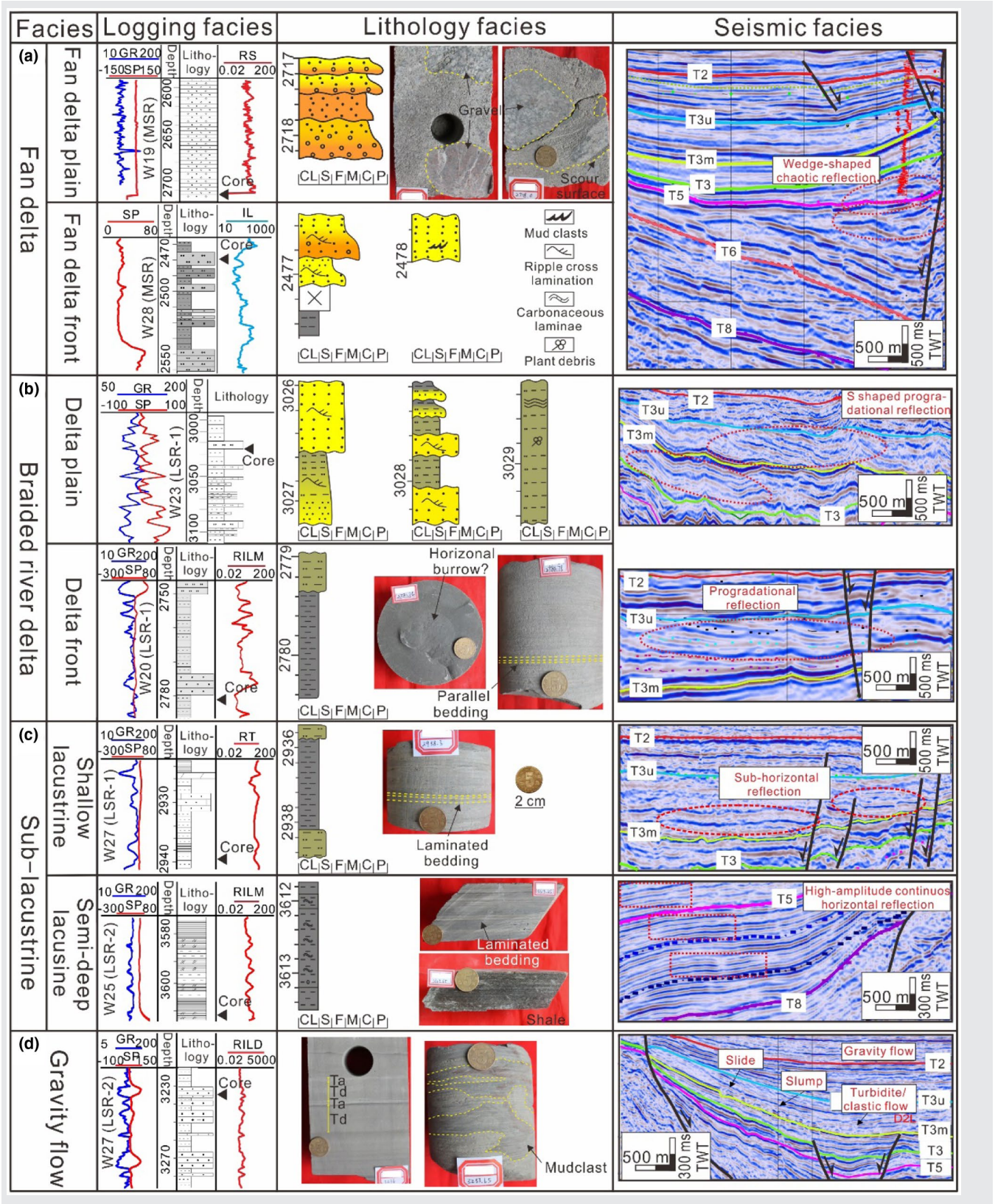

Note: The W19 (MSR) means the well name and the depth interval locates in main syn-rift stage. Drill cuttings in some wells recorded with colour but some wells only recorded lithology, but we prefer to keep this colour information.

Abbreviations: GR, natural gamma-ray log; IL, investigate induction log; LSR-1, late syn-rift stage 1; LSR-2, late syn-rift stage 2; MSR, main syn-rift; RILD, deep induction logging resistivity; RILM, medium induction logging resistivity; RS, shallow investigate double lateral resistivity log; RT, true formation resistivity; SP, spontaneous potential log.

pyroclastic facies, and subsurface elements include sill facies and conduit facies.

5.3.1 | Surficial elements

Crater facies

Description. This volcanic element appears as medium-to-high amplitude chaotic reflections in funnel- and bowl-shaped geometries that are ca. 2000 m in diameter and ca. 200 ms TWT (ca. 200 m) deep (Figures 7 and 8, and Table 4a). Drill cuttings comprise brown basaltic breccias (Figure 8 and Table 4a). Mound-shaped reflections surround these funnel-shaped areas, and drill cuttings from the mounded bodies are comprised of interbedded, medium- to thick-layered basalts (up to ca. 20 m thick), thin-layered tuffs (up to ca. 5 m thick), and rare thin-bedded volcaniclastic mudstones (ca. 5 m thick) (Figures 7 and 8, and Table 4b). On RMS amplitude maps, the funnel-shaped features are high-amplitude ovoid to circular geometries that are a few kilometres in diameter (Table 4a).

Interpretation. The funnel- and bowl-shaped geometry, brown colour basaltic breccia, and basalt lithology, together with the adjacent mounded reflections suggest this volcanic element represents strombolian explosive volcanic processes forming a crater (e.g. Kirkham et al., 2018). Volcanic explosion could result in collapse of the volcanic vent and development of craters, which are subsequently filled with basaltic breccias, giving rise to the funnel- and bowl-shaped seismic responses (e.g. Reynolds et al., 2018; Thomson, 2005; Table 4a). The funnel- and bowl-shape features could also be entirely constructional craters (e.g. Ebinghaus et al., 2014; Walker et al., 2021). These volcanic rocks show a high acoustic impedance contrast with the surrounding sedimentary rocks, resulting in the ovoid to circular RMS amplitude map geometries (Table 4a). The volcanic craters occur centrally in mounded bodies which consists of interbedded thick-layered basalts, thin-layered tuffs and mudstones, all of which gradually thinning outward from the crater centres (Table 4b).

Lava-flow facies

Description. This volcanic element is composed of low-frequency, high-amplitude chaotic wedge- or mound-shaped bodies, with a thickness of up to ca. 180 m and lateral extents of several kilometres (Figures 7 and 8, and Table 4b). They occur adjacent to, and thin rapidly away from the crater facies and, with distance away from the craters this volcanic element changes to more parallel to subparallel with surrounding reflections (Figures 7 and 8, and Table 4b). On RMS amplitude maps, this volcanic element shows medium-amplitude lobe-shaped morphologies that may become elongated away from craters (Table 4b). Drill cuttings are composed of interbedded basalt, tuff, and thick-bedded sandstones (Figures 7 and 8, and Table 4b). The gamma-ray logs of basaltic layers show box motifs, with values slightly higher (average 65 API) at the top and basal parts than the middle part (average 47 API), and resistivity logs show segmented-box shapes with high resistivity values (Table 4b).

Interpretation. The proximal wedge and mound geometries with distal lobes and sheets, interbedded basalt and tuff lithology, and elongation away from craters suggest that these volcanic elements are lava flows (e.g. Muravchik et al., 2011; Reynolds et al., 2018). During volcanic eruptions, lava flows away from craters, decreasing in thickness with distance from the eruption point, resulting in a wedge-shape or mound-shape geometry ringing craters (e.g. Manville et al., 2007). Simple lava flows are represented by high-amplitude sheet-like tabular seismic reflections, whereas compound lava flows build stacked, lobate-shaped seismic reflections that are interbedded with tuffs (e.g. Hardman et al., 2019; Jerram et al., 2009; Planke et al., 2017). The variation of gamma-ray values between top/basal and middle parts of basaltic layers probably reflects the incorporation of clastic deposits between successive eruptions, or indicates the alteration of the flow tops by weathering or interaction with subsequent eruptions (e.g. Millett et al., 2016; Planke, 1994; Table 4b).

Pyroclastic facies

Description. This volcanic element is composed of medium- to low-amplitude chaotic seismic reflections with low continuity, that mostly are stratal bounded (i.e. they conform with the overlying and underlying strata). Intervals of this volcanic element thin away from craters and typically extend over kilometres to tens of kilometres (Figures 7 and 8, and Table 4c). On RMS attribute maps, this volcanic element shows a lower amplitude and a more irregular morphology than surrounding lava-flow facies and occurs surrounding the distal parts of the lava-flow facies. Well logs display low gamma, serrated log motifs and high resistivity (Table 4c). In wells proximal to craters, drill cuttings and well logs show thick layers of tuff, with individual bed thickness ranging from ca. 3 to ca. 5 m, occasionally interbedded with thin-bedded brown-coloured volcanic breccia (ca. 5 m thick) (Table 4c). Distal to craters, well penetrations show thin-bedded tuffaceous mudstone and sandstone (ca. 0.5–2 m thick), interbedded with thick-layered mudstone and sandstone (ca. 5–10 m thick) (Table 4c).

Interpretation. The low continuity seismic reflections and interbedded breccia and tuff lithology suggest deposits

TABLE 4 *Logging- seismic facies-attribute features table of volcanic elements in the Shaleitian sub-basin*

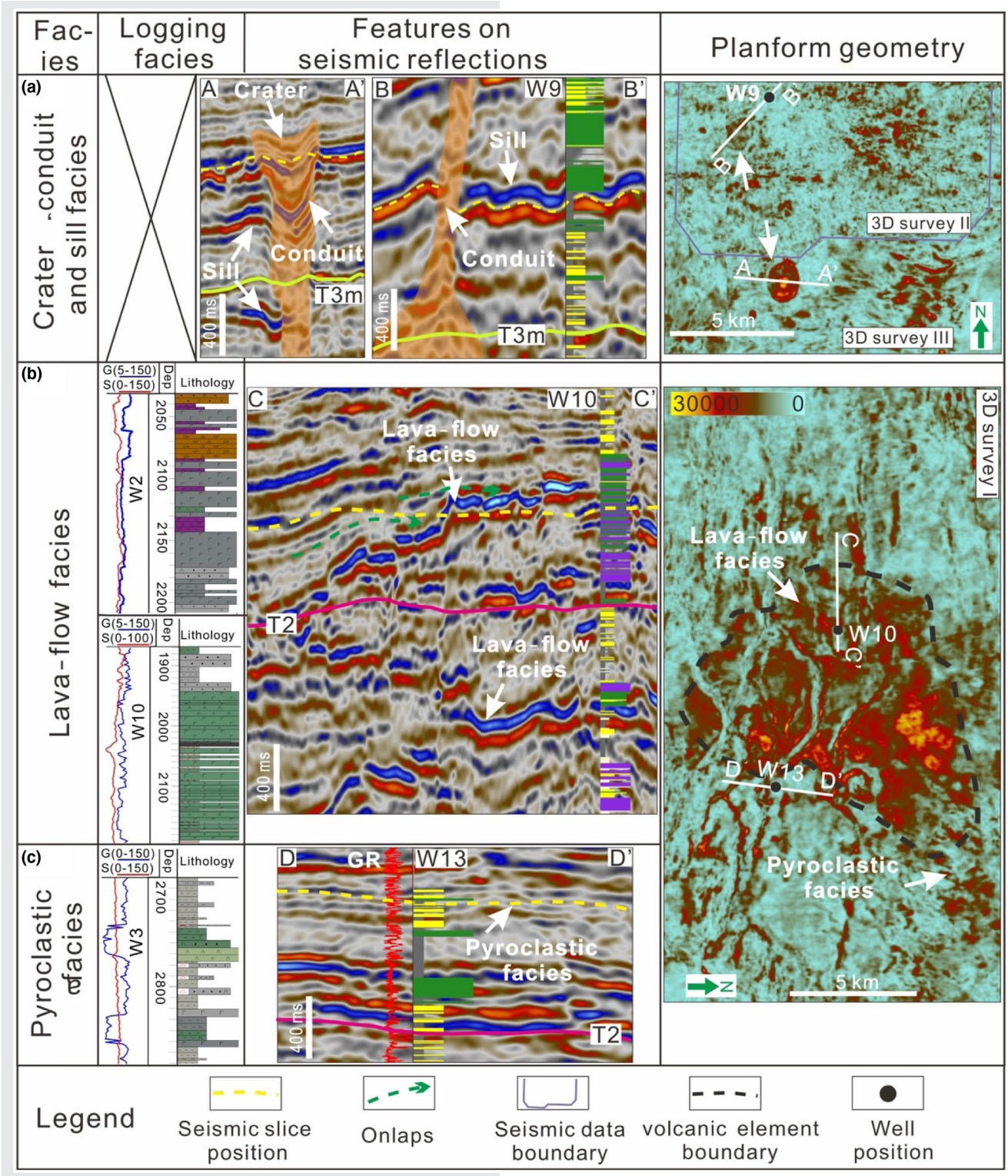

Note: Well loggings calibrate the seismic sections, and the location of seismic sections shows in seismic slices. Dotted yellow line in seismic sections marks the depth of seismic slices, and green dotted arrow marks the onlaps. Keys for drill cuttings can find in Figure 2.

Abbreviations: G, natural gamma-ray log; S, spontaneous potential log.

resulting from explosive or passive hydro-volcanic events (e.g. Kirkham et al., 2018). The wide distribution suggests atmospheric dispersion, and the interstratification with distal lava-flow facies suggests that lava flows overlap pyroclastic facies, and are subsequently buried by post-flow emplacement pyroclastic facies (e.g. Hall et al., 2013; Sulpizio et al., 2007; Table 4c). The rapid fall of erupted volcanic breccia and tuff results in a highly heterogeneous

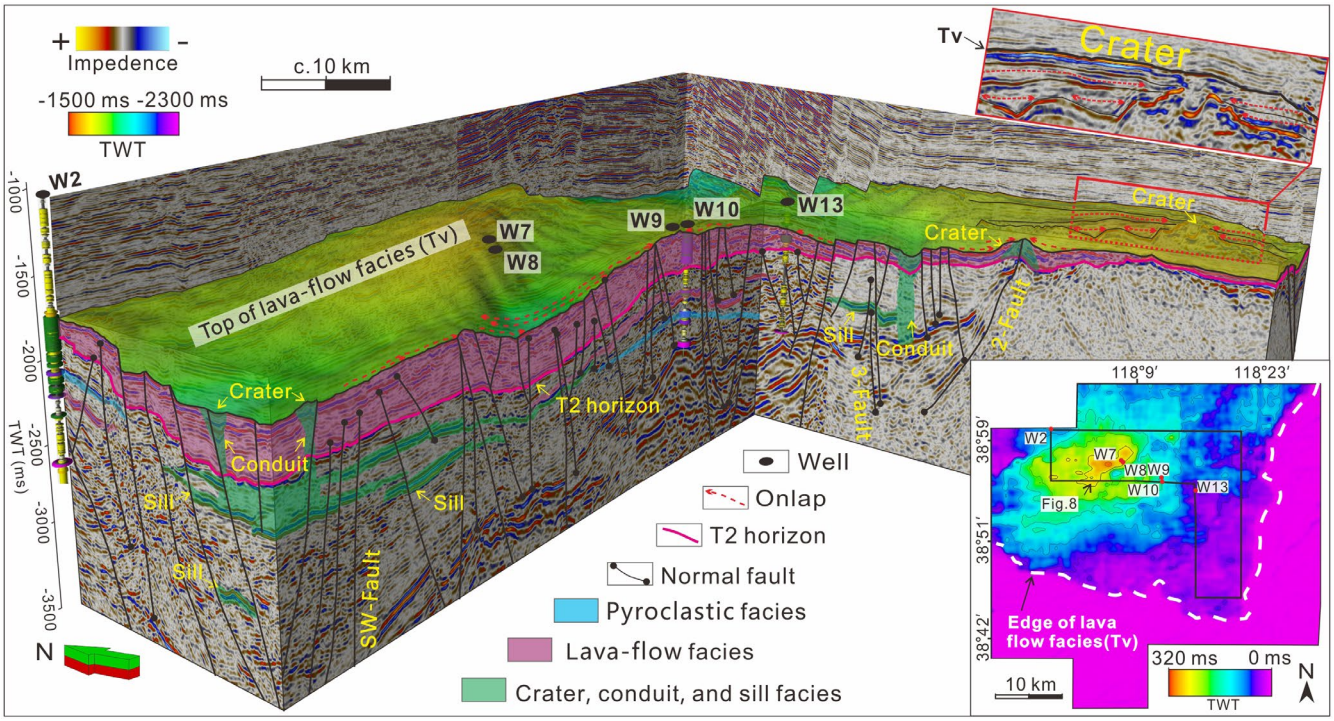

FIGURE 8 The perspective view of volcanic elements in the late syn-rift and post-rift stage. The semi-transparent yellow-green surface is the Tv surface (top of lava-flow facies). The top-right insert shows the crater features. The bottom-right insert is an isochore map between T2 and Tv horizon, showing the distribution of lava-flow facies in the post-rift stage. Note the 'L' shaped black line marks the location of the perspective view of the seismic cube. Drill cuttings and well logs of W10 and W13 indicate the volcanic topographic highs mainly consist of interbedded thick-layers basalt and thin-layers tuff. Legends for drill cuttings are shown in Figure 2

deposit that shows in seismic data as chaotic reflections with poor-continuity (e.g. Millett et al., 2021; Planke et al., 2017; Table 4c). The stratigraphic occurrence of pyroclastic facies underlying lava-flow facies suggests they mark the initiation of a volcanic eruption and may potentially be altered by subsequent lava flows (Table 4c).

5.3.2 | Subsurface elements

Conduit system

Description. This volcanic element comprises steeply dipping to sub-vertical pipe-shaped zones of medium-to-high amplitude reflectivity that cross-cut surrounding strata and extend vertically over distances of ca. 1000 ms TWT (ca. 1000 m) (Figures 7 and 8, and Table 4a). The "pipes" connect to and occur below the crater facies (Figures 7 and 8, and Table 4a). Velocity pull-up in the seismic data is also associated with these "pipe" seismic elements (Figures 7 and 8). In plan-view, they typically have irregular sub-circular geometries, 1–2 km in diameter, and with medium seismic reflectivity (Table 4a). Drill cuttings suggest lithologies comprising massive basalts.

Interpretation. The vertical connection of this volcanic element with interpreted craters and, its irregular circular geometries in plan-view and basalt lithology suggest that these pipe-like shapes are part of the sub-volcanic conduit system (e.g. Miles & Cartwright, 2010; Walker et al., 2021; Zou et al., 2008). The vertically oriented, pipe-like geometry could result from the migration of hydrothermal fluids or the migration of hydrothermal fluid-transported sediments (e.g. Grove, 2013; Reynolds et al., 2018; Svensen et al., 2006), or intrusive plugs/conduits (e.g. Jackson, 2012; Reynolds et al., 2018; Walker et al., 2021). However, the medium-to-high seismic reflectivity of these features is similar to that of the lava-flow facies and the velocity pull-up seen beneath these features indicates the pipes are seismically faster than the surrounding host rocks. These characteristics of these pipes, and their basalt lithology lead us to interpret these features as the intrusive conduits of the volcanic system (e.g. Reynolds et al., 2018; Figures 7 and 8, and Table 4a).

Sill facies

Description. This volcanic element typically consists of high continuity, high-amplitude seismic reflectors, showing a plate- and saucer-shaped cross-section, either conforming or obliquely cross-cutting surrounding strata (Figures 7 and 8, and Table 4a). In plan-view, the plate- and saucer-shapes have lengths ranging from ca. 2 km to 20 km (Figures 7 and 8, and Table 4a). Drill cuttings indicate the plate- and saucer-shaped reflections represent basalt

ranging from ca. 20 m to 100 m thick, that is overlain and underlain by mudstones (Figures 7 and 8, and Table 4a).

Interpretation. The plate- and saucer-shaped geometries, conformation with or cross-cutting of surrounding strata and basalt lithology suggest that these bodies are igneous sills. The high amplitude and high continuity of these features indicate a significant difference in lithology between these sills and their surrounding strata (e.g. Jackson et al., 2013; Magee et al., 2017; Planke et al., 2005; Walker et al., 2021). These horizontally developed, thick basaltic sills mostly encased within thick layers of mudstone, suggest that these bodies prefer to intrude relatively weak strata (e.g. Magee et al., 2014b; Magee et al., 2017; Muirhead et al., 2016; Figures 7 and 8, and Table 4a).

6 | RELATIONSHIP OF VOLCANIC ELEMENTS TO DEPOSITIONAL SYSTEMS AND BASIN STRUCTURE

6.1 | Distribution of volcanic elements in the SLT uplift and surrounding sub-basins

The overall distribution of the volcanic elements is best illustrated by the occurrence of the crater and conduit system both of which are clearly imaged as high-amplitude circular or sub-circular geometries on RMS attribute maps (Figure 9). They are well-developed on the northwestern WSLT uplift and have a close relationship to the main faults, such as the 2-Fault, 3-Fault, and NW-Fault (Figures 8–10). During the main syn-rift stage, stratigraphic records show the development of interbedded thin-layers of basalt and tuff, with the crater and conduit system accompanied by lava-flow facies mainly distributed along the 2-Fault and 3-Fault (Figures 9 and 10). In the late syn-rift stage, crater facies, conduit system, and sill facies occur further northwestward, developing along the 3-Fault and the NW-Fault. Lava-flow facies occur surrounding the crater and conduit system and fill the northern part of the Qikou sub-basin (Figures 9 and 10). Well penetrations of the late syn-rift stage 1 show it is dominantly composed of thick-layered sandstones and mudstones, while the late syn-rift stage 2 is dominated by thick layers of basalt interbedded with thin-layers of tuff, indicating volcanism mainly occurred in the late syn-rift stage 2 (Figures 9 and 10). However, the most significant volcanism occurred in the post-rift stage, with the crater and conduit system developed along the 2-Fault, 3-Fault, NW-Fault, XG-Fault, and SW-Fault, and with thick accumulations of basaltic lava-flow facies widely developed on the northwestern WSLT uplift and in the northern part of the Qikou sub-basin (Figures 9 and 10).

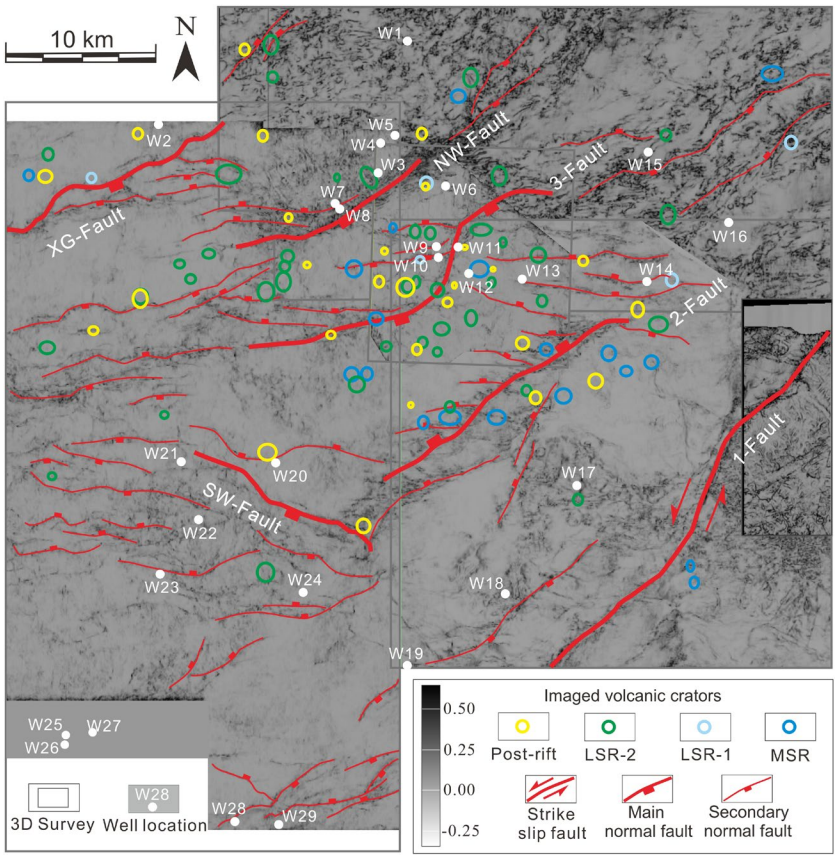

FIGURE 9 Distribution of volcanic craters and conduit systems, and fault systems in the Shaleitian sub-basin. The volcanic craters and conduit systems are drawn from 100 seismic slices (RMS attribute) that cover the main syn-rift, late syn-rift (stage 1 and stage 2), and post-rift with 25 seismic slices in each rift stage. The base map is the variance attribute slice near the T2 seismic horizon, which is used to feature the distribution of fault systems

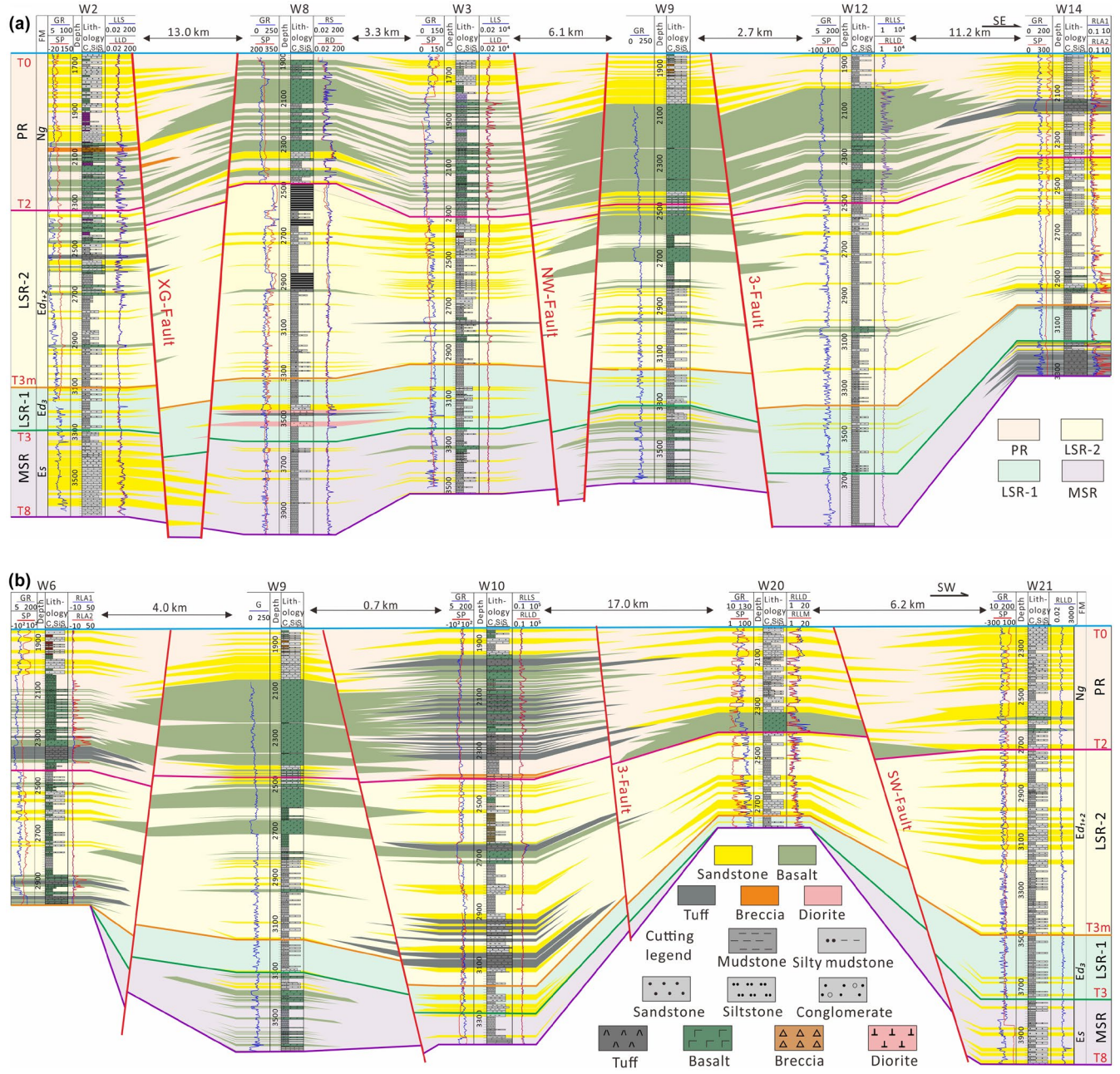

FIGURE 10 Multi-well panels showing the lateral interactions of volcanic rocks and clastic rocks in rift axis (a) and rift transverse (b) direction. Note the interactions of volcanism and depositional systems vary in different rift stages. The sections are flattened on the top of the post-rift stage (T0 horizon), and the locations of the sections are shown in Figure 4. Most of the wells did not penetrate the main syn-rift stage. FM, formation; G, natural gamma-ray log; S, spontaneous-potential log. Abbreviations for the grain size scale: C, clay; Si, siltstone; S, sandstone

6.2 | Interaction of volcanic elements and rift depositional systems

In this section, we describe the relationship between volcanic elements and rift depositional systems among the established stratigraphy for the basin. We focus on the main syn-rift stage (bounding by T8 and T3 horizons), late syn-rift stage 1 (bounding by T3 and T3m horizons), late syn-rift stage 2 (bounding by T3m and T2 horizons), and post-rift stage (bounding by T2 and T0 horizons) (Figure 3).

6.2.1 | Main syn-rift stage

Description

The time-thickness map of the main syn-rift stage has thicks developed in the Nanpu and Qikou sub-basin that

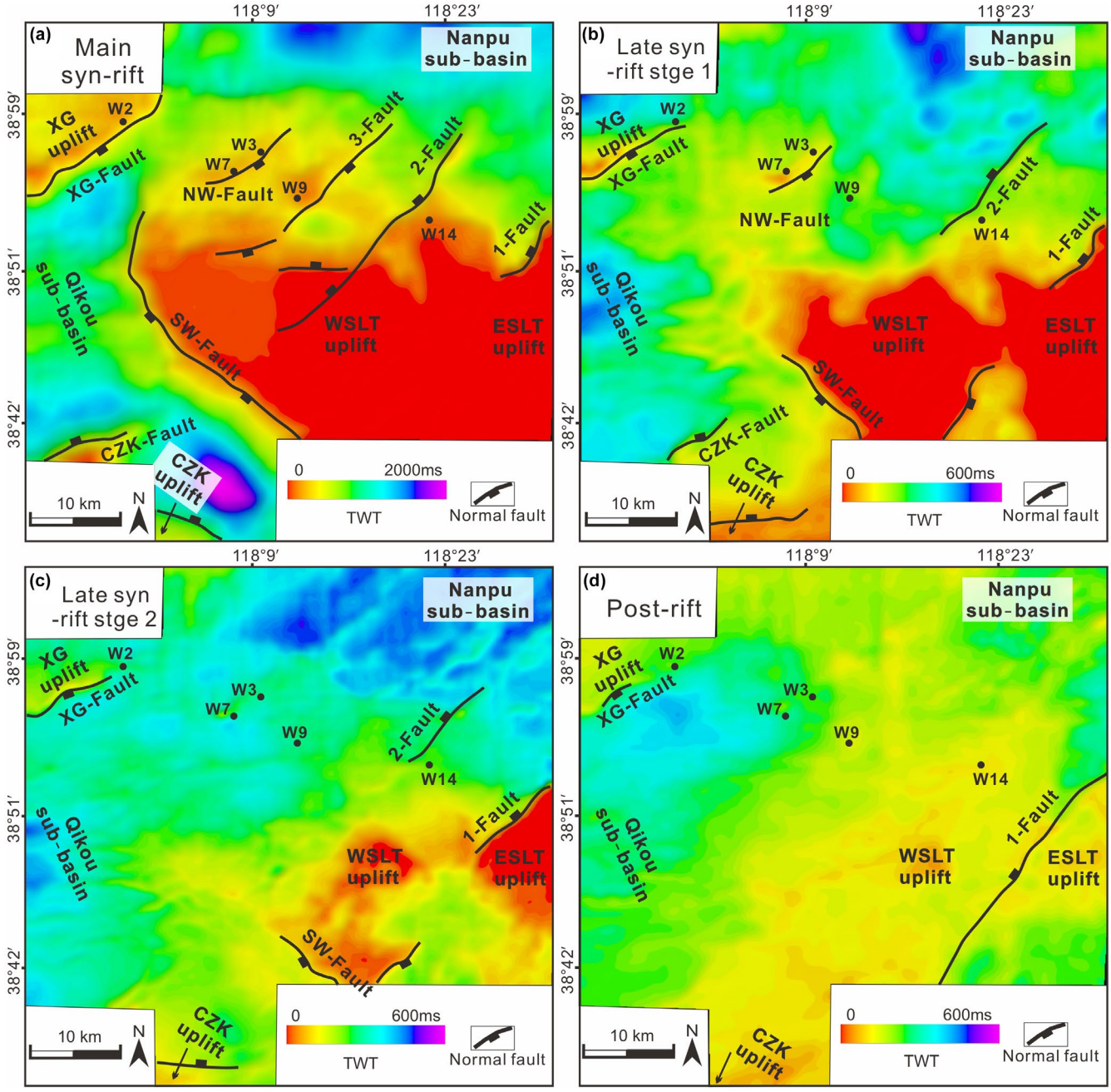

FIGURE 11 Time-domain isopach maps of different rift stages in the SLT sub-basin. Each map is shown together with fault systems. Note the SLT uplift supplied sediments into surrounding sub-basins since the main syn-rift stage and gradually decreased since the post-rift stage

range from ca. 700 ms to 2000 ms with areas ranging from ca. 60 km^2 to 100 km^2. Thin areas on the SLT uplift, XG uplift, and CZK uplift that range is <200 ms and similar thinning extend along specific boundary faults (Figure 11a). Erosional areas on the SLT uplift show up as medium amplitude, medium-high continuity RMS reflection areas, and occur where seismic units range from 0 ms to ca. 100 ms thick, with an area of about 900 km^2 (Figures 11a and 12a). The immediate hanging walls of faults are filled with medium amplitude wedge-shaped bodies of fan deltas comprising low amplitude, chaotic reflections on the RMS amplitude map (Figure 12a and Table 3a). Medium-low amplitude low-angle sigmoidal and shingled clinoforms, ca. 200 ms to 500 ms thick, of braided-river deltas occur on RMS amplitude maps as regions of elongate, low-amplitude, low-continuity reflector regions along the hanging wall dip slope of the Nanpu sub-basin (Figures 11a and 12a, and Table 3a). Within the thick areas in the Nanpu and Qikou sub-basin, distal further to fan deltas, low amplitude, low continuity, irregular

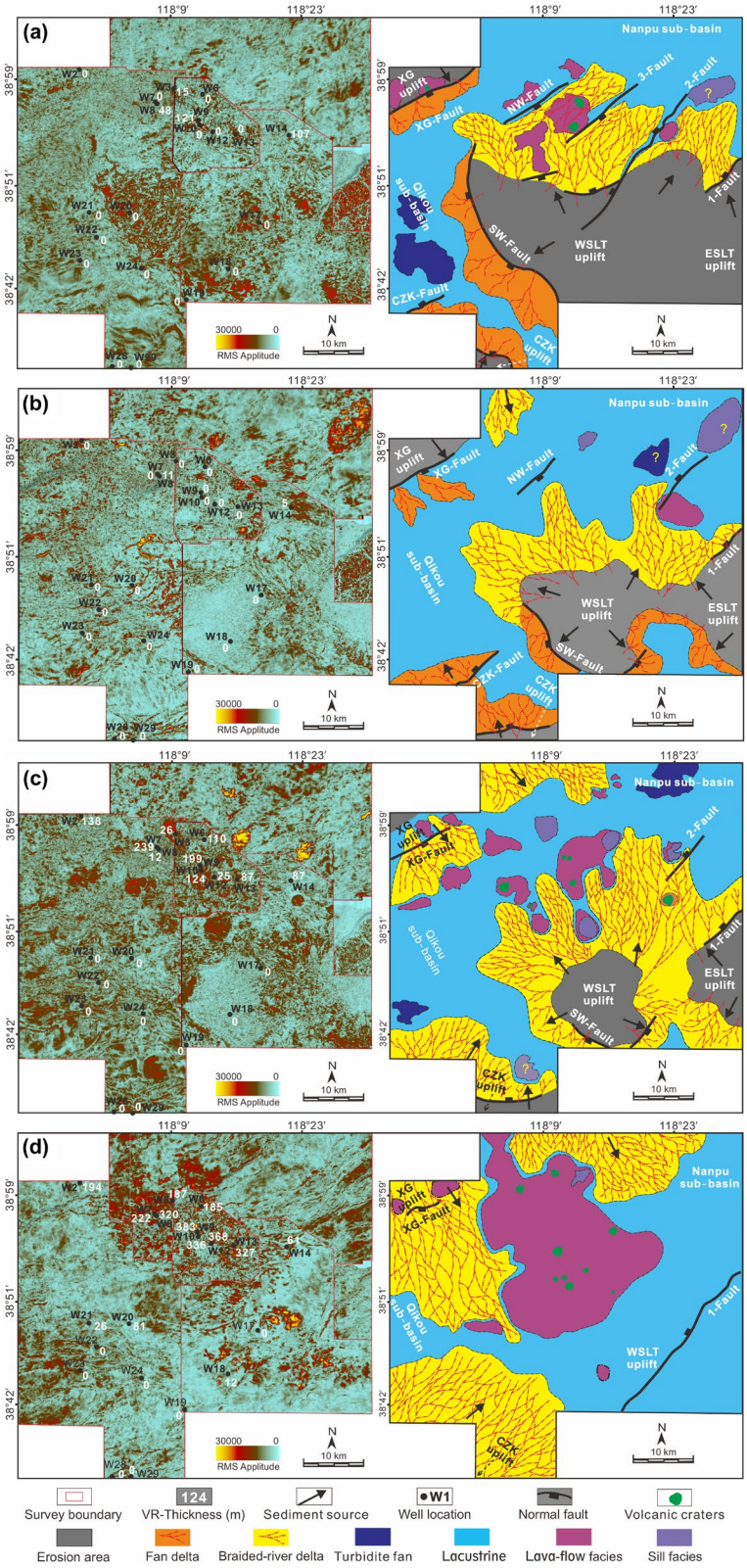

FIGURE 12 Root mean square (RMS) amplitude of seismic stratal slices and geological interpretations in different rift stages, illustrating the relationship of volcanism to basin structure and depositional systems. (a) Main syn-rift, (b) late syn-rift stage 1, (c) late syn-rift stage 2, (d) post-rift. White-colour numbers are the thickness of volcanic rocks from drill cuttings. The location of seismic slices could be found in Figure 2a

geometry bodies of gravity flow deposits occur on the RMS amplitude maps (Figures 11a and 12a). The exception being the low-medium amplitude, medium continuity potato-shaped geometries in the Qikou sub-basin (Figures 11a and 12a).

Drill cuttings suggest that this rift stage contains thin-layered basalt (mostly ca. <10 m) interbedded with sandstones (Figure 10). Thin-layered basalts occur on RMS amplitude maps as medium-high amplitude, medium-high continuity reflectors that are spatially restricted

to the fault zones of the 2-Fault, 3-Fault, and NW-Fault (Figure 12a). Volcanic elements show significant thickness variations, such as occurs in well W9, on a topographic high on the footwall of the 3-Fault which contains up to 121 m of basalt (Figures 10, 11a, and 12a). However, the limited number of wells penetrating this rift stage creates uncertainty in the assessment of their thicknesses and distribution.

Interpretation

The variety of isolated thicks and thins on the stage time-thickness map is interpreted to reflect differential fault-control subsidence and uplift and the geometry of depositional systems. The SLT uplift is the largest emergent intra-basin high, supplying sediments into surrounding sub-basins (Figure 11a). The XG and CZK uplifts developed as small emergent areas in the footwall of the XG-Fault and the CZK-Fault, respectively (Figure 12a). Portions of the sediment derived from the SLT uplift were transported northward and deposited as braided-river deltas on the dip slope and the other part of SLT uplift sourced sediments were transported southwestward and deposited as fan deltas in the immediate hanging wall of the SW-Fault (Figure 12a). Sediments from the smaller eroded uplifts are deposited in the immediate hanging wall of faults as fan deltas, with sublacustrine turbidite fans developing basinward of these fan deltas in the deepest parts of the Qikou sub-basin (Figure 12a).

Volcanic elements in this rift stage are interpreted as lava-flow facies and pyroclastic facies based on their incisive tendencies and the character of their seismic reflections. The volcanic deposits generated positive topographies that confine the dispersal of the northeastward migrating braided-river deltas off the SLT uplift (cf. Ebinghaus et al., 2014; Hardman et al., 2019; Figure 12a). Thin-layer basaltic lava flows (ca. <8 m) also occur in the hanging wall of the NW-Fault (e.g. well W9, Figure 10b). These lava flows fill the accommodation space in the immediate hanging wall of the NW-Fault and smooth out the rift-floor topography (cf. Ebinghaus et al., 2014, 2020; Figures 11a and 12a).

6.2.2 | Late syn-rift stage 1

Description

The time-thickness map of the late syn-rift stage 1 shows dramatically less variability in thicknesses than the main syn-rift stage, with thickness up to ca. 600 ms, mainly developing in the Nanpu and Qikou sub-basin (Figure 11b). Exposed erosional areas of the SLT uplift (indicated by the onlap limit of the T3 horizons) are smaller than those of the previous main syn-rift stage (Figures 2, 11b, and 12b). The most widespread area of absent and thin strata (up to ca. 30 ms thick) occurs on the SLT uplift with an area of about 500 km^2, and minor thins (ca. 100 ms) also are developed on the XG and CZK uplifts with areas up to ca. 150 km^2 (Figure 11b). In addition, local stratigraphic thins developed in the northeast of the Nanpu sub-basin and the footwall of the NW-Fault and 2-Fault (Figure 11b).

Wedge-shaped bodies in the immediate hanging wall of faults (i.e. SW-Fault and CZK-Fault) show low amplitude, medium-high continuity fan-shaped geometries on the RMS amplitude map (Figure 12b). Along the northern dip slope of the SLT uplift, medium amplitude, medium continuity, relatively straight channel-shaped geometries develop in a zone of ca. 30 km wide, fringing the SLT uplift, with low amplitude, low continuity elongate geometries further basinward (Figure 12b). Similar elongate amplitude geometries are also developed to the northeast of the XG uplift and extend southward into the Nanpu sub-basin (Figure 12b).

Wells penetrating this stage show thick mudstone intervals (up to ca. 150 m) in the mapped thicks of the Nanpu and Qikou sub-basins (Figure 12b). Drill cuttings suggest very few penetrations of igneous rock, except for 5 m of interbedded basalt and tuff in well W14 on the footwall of the 2-Fault that generates the medium-high amplitude and medium continuity anomalies on RMS amplitude maps (Figures 10 and 12b). The RMS amplitude map of this stage shows similar high amplitude, high continuity, ellipse-shaped and irregular-shaped geometries developed in the Nanpu sub-basin and on the northern dip slope of the SLT uplift (Figure 12b).

Interpretation

The time-thickness map of this stage indicates the SLT uplift was still a prominent structural high at this time and continued to supply sediments into the surrounding depocentres (Figure 12b). Wedge-shaped bodies in the immediate hanging walls of faults are interpreted as fan deltas, and clinoforms on the northern dip slope of the SLT uplift indicate the development of braided-river deltas in this region (Figure 12b). The thick mudstones deposited in sub-basins represent low energy sub-lacustrine environments (Xu et al., 2008; Zhu et al., 2015; Figure 10b). Drill cuttings and seismic geomorphologies suggest sparse development of surficial volcanic elements, however small-scale lava-flow facies found around well W14, prove the exception (Figures 10 and 12b). Seismic geomorphological features suggest an intrusive origin (conduit system and sill facies) for volcanic rocks in this rifted stage (cf. Planke et al., 2005; Walker et al., 2021; Figure 12b).

6.2.3 | Late syn-rift stage 2

Description

The SLT uplift continued to be the main thin area of strata; about 40 ms in thickness, with minor thins <ca. 100 ms, occurring on the XG and CZK uplifts (Figure 11c). Erosional areas (ca. 300 km^2) on the SLT uplift correspond to areas of low amplitude, medium-high continuity reflection, and within this rift stage have become isolated; with separate areas on the WSLT and ESLT uplift (Figure 12c).

Medium amplitude, medium continuity, chaotic reflections fringing the SLT uplift and pass basinward to low amplitude, low continuity reflections with elongate low amplitude anomalies in map view (Figure 12c). Similar transition features also develop in the hanging wall of the XNZ-Fault, XG-Fault, and CZK-Fault, and into the Nanpu and Qikou sub-basin (Figures 1 and 12c). Well penetrations show interbedded thin-layered basalt and tuff (average ca. 10 m thick) throughout this rift stage, with the thickest development of 239 m in well W7, in the footwall of the NW-Fault (Figures 9, 10 and 12c). In distal parts of the dip slope of the SLT uplift, thin-layer interbedded basalts and tuffs, appearing in RMS amplitude maps as medium-to-high amplitude, high continuity reflector packages with sub-circular and irregular-shaped planform, interfringe with clastic sediments (e.g. in wells W2 and W7; Figures 10 and 12c).

Interpretation

Even though the total exposed area of the SLT uplift is reduced in this rift stage, it still represents the largest intra-basin high in the study area, and continues to supply sediment to surrounding sub-basins (Figure 12c). Braided-river deltas are developed around the SLT uplift and extend northward off the dip slope of the SLT uplift into the Nanpu sub-basin (Figure 12c). During this time, the Yanshan fold-belt sediment source supplied sediment to axial braided-river deltas that prograded to the southeast into the Nanpu and Qikou sub-basins (Liu, 2016; Liu et al., 2017; Figures 1 and 12c). Drill cuttings and seismic geomorphology suggest volcanic topography in the basins constructed from the crater, lava flow, and pyroclastic facies. These constructive volcanic highs cause bifurcation and deflection of the distal parts of the NNW-prograding braided-river deltas on the dip slope of the SLT uplift (Figures 9 and 12c). The close lateral association of lava flows and pyroclastic facies with braided-river deposits emphasises the importance of volcanic elements in the geomorphology of these landscapes (Figure 10). Similar examples of diversion of depositional systems by volcanic landform occur in the Miocene Columbia River Basalt Province (Ebinghaus et al., 2014, 2020; Hardman et al., 2019).

6.2.4 | Post-rift stage

Description

The post-rift stage time-thickness varies from ca. 50 ms to ca. 450 ms, with thicks (ca. 350–450 ms) developed in the Qikou and Nanpu sub-basins and thins (ca. 50–100 ms) locally occurring on the SLT, XG, and CZK uplifts (Figure 11d). The exposed areas on the SLT uplift were onlapped and overstepped and post-rift stage sediments were deposited conformably on the basal-boundary T2 horizon (Figure 2). Medium-low amplitude low-angle sigmoidal and shingled clinoforms, with individual clinoform foresets typically ca. 150 ms in height, are widely developed in the northern Nanpu and southwestern Qikou sub-basins and prograde southeastward (Figures 2 and 12d). Clinoforms sourced from the CZK uplift, are also developed in the southwestern Qikou sub-basin and prograde northeastward (Figures 2 and 12d). These clinoform units occur as low amplitude, medium-low continuity elongate geometries in map view. Basinward of these elongate geometries low amplitude, medium-high continuity, low amplitude reflections correspond to thick successions of mudstone in wells that penetrate this stage (Figures 10 and 12d).

Drill cuttings through these intervals show thick-layered basalt interbedded with thin-layered tuff, with individual layer thicknesses ranging between ca. 5 m to ca. 35 m and cumulative thickness ranging from 187 m in well W3 to 383 m in well W9 (Figures 10 and 12d). Medium-high amplitude, medium continuity irregular shapes on the RMS amplitude map represent lava-flow facies. The extensive occurrence of craters and lava flows results in volcanic topographic highs of ca. 20 km long and ca. 15 km wide sitting in the northwest of the study area (Figures 2b, 8, 10, and 12d), and the top surface of these thick-layered basalts; the Tv horizon, is onlapped by younger clastic strata (Figures 2b, 8, and 10).

Interpretation

The deposition of post-rift strata upon regional and localised uplifts and the lower variability of the time-thickness map of this rift stage suggests reduced fault activity and the likely submergence of the SLT, XG, and CZK uplifts. As a result, no intra-basin highs supplied sediment into adjacent depocentres during the post-rift stage. The propagation directions of clinoforms indicate sediments mostly originated from extrabasinal sediment sources to the northwest and southwest (Figures 2 and 11d), suggesting sediment was derived from the Yanshan fold-belt (Xu et al., 2008; Zhang, 2000; Figure 1). Sediments from these sources fed large-scale braided-river deltas that prograded southeastward; parallel to the rift axis, and northeastward; oblique to the rift axis (Figures 11d and 12d). Lava flows

and pyroclastic facies occur widely throughout this stage, resulting in isolated volcanic highs, which caused the separation of the southeastward prograding axial braided-river deltas (Figure 12d).

7 | DISCUSSION

In this section, we discuss some of the implications of the volcanism and clastic depositional records in the SLT uplift and surrounding sub-basins, focusing on the volcanism occurrence and influences in rift basin tectono-sedimentation. In addition, we present a volcano-sedimentary model that highlights the interactions of volcanism and clastic sedimentation that can be used more generally in volcanic rift basins.

7.1 | Structural controls on the spatial distribution of extrusive centres

The geometry and evolution of rift basins are mainly controlled by the activity of basin boundary and intra-basin faults which in turn is controlled by the lithology and structure of the crust and lithosphere (e.g. Gawthorpe & Leeder, 2000; Huismans & Beaumont, 2011, 2014; Ravnas & Steel, 1998). However, in volcanic rifts, the controls on the location and intensity of volcanism remain unclear. Schofield et al. (2017), based on a 3D seismic reflection data-based study of the Palaeogene Faroe-Shetland Sill Complex in the Faroe-Shetland Basin, suggested the main magma input zones into the basin were controlled primarily by the NE-SW basin structure. Jolley et al. (2021) also suggested volcanic activity was initially concentrated on basin flank structures. Similar to the Faroe-Shetland Basin, the NE-striking basement-involved faults in this study, such as the 2-Fault, 3-Fault, NW-Fault, and XG-Fault, appear to control the location of most volcanic conduit systems and craters (Figures 2b, 8, and 9). Thus we suggest major normal faults have a control on location of eruptive centres.

7.2 | Volcanic modification of rift topography and its influence on clastic depositional systems

Several studies shown that sudden input of lava flows or pyroclastic material may significantly change local rift drainage networks and depositional systems (e.g. Grove, 2013; Hardman et al., 2019; Hole et al., 2013; Sulpizio et al., 2007). Flowing lava will naturally seek out existing topographical lows, which in these settings are often the hanging walls of rift bounding normal faults (e.g. Millett et al., 2021; Schofield & Jolley, 2013; Zanchetta et al., 2004). D'Elia and Martí (2013), working in the Lower and Upper members of the Sañicó Formation of the Jurassic Neuquén basin, Argentina, suggested that thick lava units deposited in the immediate hanging wall of the basin's boundary faults reduced topography within rift depocentres. In the Kamasia region of the Kenya Rift, a large volume of volcanic extrusives (ca. 220,000 km^3) infilled hanging wall depocentres, creating shallow ephemeral lacustrine basins (Baker, 1986; King & Chapman, 1972). This tectonic geomorphology differs fundamentally from many of the other rift basins in the East African Rift which are typically deep, long-lived lakes with thick sedimentary successions, such as those of Malawi and Turkana Rifts (Baker, 1986; Schofield et al., 2021). Such topographic "healing" is not limited to the margins of the rifts. In the Reykjanes Peninsula, Iceland in February 2021, the continuous eruption of the Fagradalsfjall volcano resulted in the filling of the Geldingadalir valley by lava flows. Results from the SLT uplift and surrounding basins indicate volcanic processes occurring in the Neogene early post-rift stage of the SLT and surrounding basins infilled pre-existing topography in the northern Qikou sub-basin, to an average thickness of ca. 250 m (Figures 8, 11d, and 12d). In the Palaeogene syn-rift stage in sub-basins that surround the SLT uplift, seismic facies suggest that volcanic elements preferably infill rift accommodation, reducing intra-rift basin topography.

Volcanism can also build significant topographic highs, modifying regional drainage patterns and altering depositional system dynamics and distributions (e.g. Hardman et al., 2019; Hole et al., 2013; Magee et al., 2013; Magee et al., 2017; Schofield & Jolley, 2013). Focusing on the Old Red Sandstone Basin, NE Scotland, Hole et al. (2013) documented the construction of a lava field which led to the development of a local topography of sufficient height to divert the fluvial drainage system away from the lava field. Results from this study indicate lava flows formed a NE-SW elongate mounded topography, ca. 16 km long and ca. 8 km wide, and up to ca. 320 m high on the relatively flat T2 horizon parallel to the NW-Fault (Figures 8, 10, and 11d). These topographic highs split and divert these southeastward prograding axial braided-river deltas (Figure 11d). In addition to various volcanic flows affecting depositional topography, the incremental emplacement of subsurface sill intrusions is also known to influence the subaerial topography (e.g. Hartley et al., 2011; Magee et al., 2013, 2017; Walker et al., 2021). However, no clear examples of sill emplacement influencing depositional topography are recognised in this study.

Finally, the interaction between episodic volcanism and clastic depositional systems is a symbiotic process. In the rifted Jangki basin of SE Korea, Bahk and Chough (1996) noted that during volcanic eruptions, dacitic and basaltic volcanoclastic aprons spread downslope impinging on the rift's axial fluvial system, while during inter-eruptions periods, fluvial systems recovered and eroded the distal toes of these volcanoclastic aprons (Bahk & Chough, 1996). Schofield and Jolley (2013) suggested that sustained periods of volcanic hiatus provide sufficient time for establishing new drainage networks or for the recovery of previous drainage networks. Meanwhile, high eruption rate periods may quickly establish more localised drainage and deposit sedimentary interbeds within volcanic records (e.g. Ebinghaus et al., 2014, 2020; Schofield & Jolley, 2013). The relative timescales of eruption and inter-eruption periods need to be unwoven to fully understand complex interplays of volcanic and sedimentary processes in volcanic rifts.

7.3 | Influences of volcanic sediment input on clastic depositional systems

Volcanically active basins experience sediment supply rates orders of magnitude greater than those of non-volcanic active basins (e.g. Fisher & Smith, 1991; Houghton & Landis, 1989; Manville et al., 2009; Vessell & Davies, 1981). Volcanic processes supply a large volume of volcanic-denued sediment, ranging from gravel to clay grade, into syn- and post-eruptive clastic depositional systems (e.g. D'Elia & Martí, 2013; Millett et al., 2021; Planke et al., 2000; Schofield & Jolley, 2013). In this study petrographic analysis indicates that igneous rock debris comprises between 46% and 97% (average of 68%) of all the rock fragments in preserved sediments of the main syn-rift (Eocene) and late syn-rift (Oligocene) stages (Figure 6). This dominance of volcanic-derived clasts occurs despite the largest intra-basin sediment source area, the SLT uplift, being mainly composed of metamorphic and carbonate rocks (e.g. Liu et al., 2017; Zhang, 2000). Such contributions have been noted in other basins as well, for example, D'Elia and Martí (2013) indicated that the Jurassic Sañicó Formation in the Neuquén Basin contains up to 72% volcanic clasts.

High rates of sedimentation and the coarse nature of the debris, coupled with the tectonic activity in these basins inevitably generates unstable landscapes and increase the probability of landslides (e.g. Planke et al., 2017; Schofield & Jolley, 2013). These landslides not only contribute sediment to the system but also create landscapes that are "out of grade" (e.g. Prather, 1998), driving rivers to shift their courses, shorelines to alter, and slopes to persist in long periods of re-grading to more stable geometries. Miyabuchi (1999) documented the occurrence of a subaerial debris avalanche along the volcanic Mayuyama Massif, Japan, that shifted a 3 km long stretch of coastline seaward by 600 m. Planke et al. (2017) imaged the occurrence of volcanogenic debris flows and large slump blocks along the prominent Vøring rift escarpment in the NE Atlantic which formed when lava flows reached the coastline. In the Palaeogene SLT uplift and surrounding sub-basins, turbidite fans are more developed in the late syn-rift stage 2, which is associated with more volcanism compared to the late syn-rift stage 1 (Figure 12b,c). It is possible that the frequency and magnitude of eruptions resulted in a high rate of volcanic sediment supply during the late syn-rift stage 2, although a variety of factors can influence the development of such fans (e.g. Hardman et al., 2019; Millett et al., 2021). Besides, volcaniclastic materials often exist as unstable mineral phases that will diagenetically alter, degrading porosity and permeability. Such changes have a dramatic effect on exploration reservoir risk of any intra-basaltic prospects (e.g. Helland-Hansen et al., 2009; Schofield & Jolley, 2013).

7.4 | Interactions of rift volcanism and clastic depositional systems in rifts: a generic model

By integrating a variety of models of volcanism (e.g. Bahk & Chough, 1996; Cole & Ridgway, 1993; D'Elia & Marti, 2013; Planke et al., 2000, 2017; Riggs et al., 1997) with tectono-sedimentary models of rift basins (e.g. Gawthorpe & Leeder, 2000; Ravnas & Steel, 1998), and infusing the observations presented in this paper, we propose a generic volcano-sedimentary model of rift basin evolution focusing on the interactions of volcanism and clastic sedimentation during the syn-rift and early post-rift (Figure 13).

In the early part of the syn-rift stage, depocentres initially develop in the hanging wall of isolated fault segments (Gawthorpe & Leeder, 2000). Volcanic eruptions may provide a high amount of volcanic debris to isolated syn-rift depocentres that enhances filling of hanging wall topographic lows by lava and pyroclastic flows (e.g. Baker, 1986; D'Elia et al., 2018; Hole et al., 2013; Figure 13a). As a result, basement highs between syn-rift depocentres (e.g. segment boundaries between half grabens) may be more easily breached, enabling drainage integration and enhancing axial sediment transport (Figure 13a). In contrast, local volcanic topographic highs, within isolated depocentres, may cause diversion and splitting of transverse fan and deltaic systems (e.g.

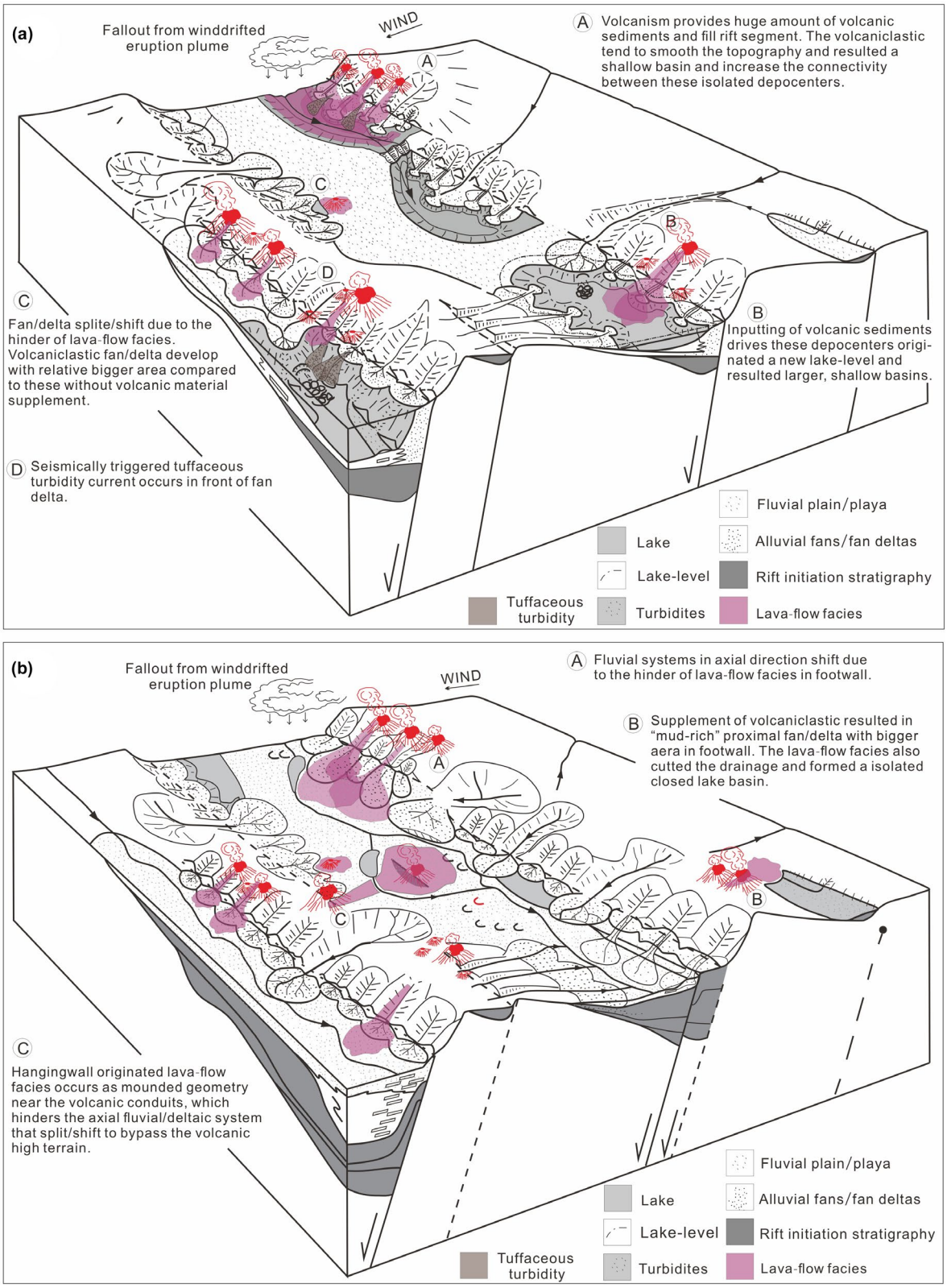

FIGURE 13 A generic model showing the interactions of volcanism and clastic depositional systems in the syn-rift stage (a) and post-rift stage (b). The original basin structures and depositional systems were cited from Gawthorpe and Leeder (2000) and not to scale

Hardman et al., 2019; Millett et al., 2021; Planke et al., 2017; Figure 13a). During periods of volcanism hiatus, new drainage networks may establish or previous drainage networks may recover (e.g. Ebinghaus et al., 2020; Schofield & Jolley, 2013; Figure 13a). Volcanic-induced earthquakes may also trigger sediment failure,

increasing the frequency of slumps and slides into the immediate hanging wall depocentres (e.g. Fisher & Smith, 1991; Hayes et al., 2002; Planke et al., 2017; Umazano et al., 2014; Figure 13a).

In the later part of the syn-rift stage and early post-rift stage, depocentres enlarge and coalescence following fault segment growth and linkage (Gawthorpe & Leeder, 2000). During this rift stage, rift topographic rugosity will gradually decrease, resulting in increased drainage coalesence and increased axial flow of fluvial systems in the basin. In the immediate hanging wall of normal faults, footwall-sourced lava flows and pyroclastic flows infill the topographic lows, pushing axial fluvial systems away from the immediate hanging wall (Figure 13b). Lava and pyroclastic flows may also dam axial drainages and result in local, small-scale lakes (e.g. Hardman et al., 2019; Williamson & Bell, 2012; Figure 13a). Also, in hanging wall depocentres, the building of volcanic topographic highs during eruptions may split and divert axial fluvial and deltaic systems and transverse fan and deltaic systems (Figure 13b). In contrast, during inter-eruption phases, axial fluvial systems may breach these volcanic topographic highs (Bahk & Chough, 1996; Figure 13b).

In general, volcanism in rift basins results a wide range of impacts on sediment routing systems. Such impacts include: (1) enhancing sediment dispersal by smoothing out fault induced topographic rugosity, and (2) creating topographic barriers, resulting in damming depocentres which may block routing system and create local lakes, or creating local barriers that divert sediment routing systems. In addition, volcanism increases sediment supply compared to non-volcanic rift settings resulting in increased sediment accumulation, possible increases in gravity failures (slumps, slides, and debris flows). Even though volcanism can significantly modify basin topography and depositional systems in rift basins, we should note the interaction between episodic volcanism and clastic depositional systems is a mutual process and tectonics still dominate the overall tectono-sedimentary evolution in rift basins.

8 | CONCLUSION

This study of the Palaeogene-Neogene Shaleitian Uplift and surrounding sub-basins of the Bohai Bay Basin, China offers a well-documented subsurface (seismic, logs and core) example of a volcanic rift basin, that allows the interactions between volcanism and clastic sedimentation in rift basins to be investigated. Our results reveal that:

1. Steeply dipping basement-involved intra-basin faults control the spatial distribution of the volcanic conduit system during the syn- and post-rift stages. The faults continue to act as magma conduits once displacement accrual has stopped along the faults.
2. During the syn-rift stage the SLT uplift supplied basement-derived sediment to surrounding sub-basins developing transverse fan deltas and braided-river deltas. Volcanism mainly occurred as small-scale crater facies, thin lava flows, and intrusive sills. During the post-rift stage, the SLT uplift was progressively inundated, reducing the area being eroded and the associated transverse depositional systems gradually shrink in size. Large-scale axial braided-river deltas are fed by sediments originating from the Yanshan fold-belt to the northwest. Volcanism in the post-rift stage was mostly recorded as large-scale craters and thick lava-flow facies.
3. Volcanism significantly modifies the rift topography in the sub-basins surrounding the SLT uplift. During the early part of the syn-rift stage, volcanic deposits partially infill rift topographic lows, reducing topographic rugosity and increasing the along-strike connectivity of syn-rift depocentres. This volcanic-sedimentary interaction enhances the breaching of basement highs between isolated syn-rift depocentres and increasing the integration of through-flowing axial depositional systems. During the later part of the syn-rift stage and the early part of the post-rift stage, lava and pyroclastic flows partially infill the remaining topographic lows in the immediate hanging wall and locally dam axial fluvial systems and form localised lakes. Volcanic topographic highs associated with NE-striking intra-basin faults split and divert axial and transverse depositional systems.
4. Volcanic eruptions supply significant volumes of volcanic sediment to clastic depositional systems. Enhanced sediment supply increases the progradation of clastic depositional systems and increases sedimentation rates compared to non-volcanic rift settings. In contrast, clastic depositional systems developed during inter-eruptions phases contain relatively lower volumes of volcanic sediment and have relatively lower sedimentation rates. Volcanic activity results in unstable subaerial and subaqueous slopes and deposits, increasing the occurrence of landslides.

This study highlights the importance of volcanism and volcanic landforms on sediment routing systems, depositional systems, and sedimentation rates in rift basins. The generic volcanic-tectono-sedimentary model developed in this study also emphasises the interactions of volcanism and clastic depositional systems, advancing current tectono-sedimentary models of rift basins.

ACKNOWLEDGEMENTS

This research was funded by the Major National Science and Technology programs in the "Thirteenth Five" plan period (No: 2017ZX05001002) and also supported by the 111 project (B20011). Gawthorpe acknowledges the award of the VISTA Professorship from the Norwegian Academy of Science and Letters which also funded a visiting scholarship to Chen. We would like to thank the editor, Dr Craig Magee, reviewers Drs John Millett, Qiliang Sun, and Amanda Owen for their contributed comments which significantly improved this manuscript. We also would like to thank Drs Ebinger, Leandro D'Elia, and an anonymous reviewer for their comments on the early versions of this manuscript. The authors also thank Drs Pengfei Hou, Haipeng Li, and Hang Deng at the Colorado School of Mines for insightful discussions. In addition, we appreciate the Bohai Oil Field Research Institute, Tianjin Branch of CNOOC for their support and permission to publish this paper.

CONFLICT OF INTEREST

We are not aware of any conflicts of interest relating to this work.

PEER REVIEW

The peer review history for this article is available at https://publons.com/publon/10.1111/bre.12651.

DATA AVAILABILITY STATEMENT

The data that support the findings of this study are available from Bohai Oil Field Research Institute, Tianjin Branch of CNOOC. Restrictions apply to the availability of these data, which were used under licence for this study. Data are available from the author(s) with the permission of Bohai Oil Field Research Institute, Tianjin Branch of CNOOC.

ORCID

Hehe Chen https://orcid.org/0000-0003-0312-0764
Robert L. Gawthorpe https://orcid.org/0000-0002-4352-6366

REFERENCES

Abdelmalak, M. M., Planke, S., Polteau, S., Hartz, E. H., Faleide, J. I., Tegner, C., & Myklebust, R. (2019). Breakup volcanism and plate tectonics in the NW Atlantic. *Tectonophysics*, *760*, 267–296.

Acocella, V. (2014). Structural control on magmatism along divergent and convergent plate boundaries: Overview, model, problems. *Earth-Science Reviews*, *136*, 226–288.

Allen, M. B., Macdonald, D. I. M., Xun, Z., Vincent, S. J., & Brouet-Menzies, C. (1997). Early Cenozoic two-phase extension and late Cenozoic thermal subsidence and inversion of the Bohai Basin, northern China. *Marine and Petroleum Geology*, *14*(7–8), 951–972.

Bahk, J. J., & Chough, S. K. (1996). An interplay of syn-and interruption depositional processes: The lower part of the Jangki Group (Miocene), SE Korea. *Sedimentology*, *43*(3), 421–438.

Baker, B. H. (1986). Tectonics and volcanism of the southern Kenya Rift Valley and its influence on rift sedimentation. *Geological Society, London, Special Publications*, *25*(1), 45–57.

Blair, T. C., & McPherson, J. G. (1994). Alluvial fans and their natural distinction from rivers based on morphology, hydraulic processes, sedimentary processes, and facies assemblages. *Journal of Sedimentary Research*, *64*(3a), 450–489.

Cole, R. B., & Ridgway, K. D. (1993). The influence of volcanism on fluvial depositional systems in a Cenozoic strike-slip basin, Denali fault system, Yukon Territory, Canada. *Journal of Sedimentary Research*, *63*(1), 152–166.

D'Elia, L., & Martí, J. (2013). Caldera events in a rift depocentre: An example from the Jurassic Neuquén basin, Argentina. *Journal of the Geological Society*, *170*(4), 571–584.

D'Elia, L., Martí, J., Muravchik, M., Bilmes, A., & Franzese, J. R. (2018). Impact of volcanism on the sedimentary record of the Neuquén rift basin, Argentina: Towards a cause and effect model. *Basin Research*, *30*, 311–335.

Dickinson, W. R., Beard, L. S., Brakenridge, G. R., Erjavec, J. L., Ferguson, R. C., Inman, K. F., & Ryberg, P. T. (1983). Provenance of North American Phanerozoic sandstones in relation to tectonic setting. *Geological Society of America Bulletin*, *94*(2), 222–235.

Du, J. X., Shi, W. W., Zhou, H., Wang, Q. L., Xia, Q. J., & Liu, J. R. (2014). Zircon U-Pb age and formation model of volcanic rocks from Nanpu Sag of Bohai Bay Basin. *Oil and Gas Geology*, *35*, 742–747.

Duncan, L. J., Dennehy, C. J., Ablard, P. M., & Wallis, D. W. (2020). The rosebank field, blocks 213/27a, 213/26b, 205/1a and 205/2a, UK Atlantic margin. *Geological Society, London, Memoirs*, *52*(1), 980–989.

Ebinger, C., & Scholz, C. A. (2012). *Continental rift basins: The East African perspective* (pp. 183–208). Tectonics of Sedimentary Basins: Recent advances.

Ebinghaus, A., Hartley, A. J., Jolley, D. W., Hole, M., & Millett, J. (2014). Lava–sediment interaction and drainage-system development in a large igneous province: Columbia River Flood Basalt Province, Washington State, USA. *Journal of Sedimentary Research*, *84*(11), 1041–1063.

Ebinghaus, A., Taylor, R., Barker, A., Hartley, A. J., Jolley, D. W., & Hole, M. J. (2020). Development of inter-lava drainage systems in LIPs: The Columbia River Flood Basalt Province (USA) as a case study. *Journal of Sedimentary Research*, *90*(10), 1346–1369.

Famelli, N., Millett, J. M., Hole, M. J., Lima, E. F., Carmo, I. D. O., Jerram, D. A., & Howell, J. A. (2021). Characterizing the nature and importance of lava-sediment interactions with the aid of field outcrop analogues. *Journal of South American Earth Sciences*, *108*, 103108.

Ferguson, D. J., Barnie, T. D., Pyle, D. M., Oppenheimer, C., Yirgu, G., Lewi, E., & Hamling, I. (2010). Recent rift-related volcanism in Afar, Ethiopia. *Earth and Planetary Science Letters*, *292*(3–4), 409–418.

Fisher, R. V., & Smith, G. A. (Eds.). (1991). *Sedimentation in volcanic settings (No. 12240)*. Sepm Society for Sedimentary.

Gawthorpe, R. L., & Leeder, M. R. (2000). Tectono-sedimentary evolution of active extensional basins. *Basin Research*, *12*(3–4), 195–218.

Gawthorpe, R. L., Leeder, M. R., Kranis, H., Skourtsos, E., Andrews, J. E., Henstra, G. A., & Stamatakis, M. (2018). Tectono-sedimentary evolution of the Plio-Pleistocene Corinth rift, Greece. *Basin Research*, *30*(3), 448–479.

Grove, C. (2013). Submarine hydrothermal vent complexes in the Palaeocene of the Faroe-Shetland Basin: Insights from three-dimensional seismic and petrographical data. *Geology*, *41*(1), 71–74.

Hall, M. L., Steele, A. L., Mothes, P. A., & Ruiz, M. C. (2013). Pyroclastic density currents (PDC) of the 16–17 August 2006 eruptions of Tungurahua volcano, Ecuador: Geophysical registry and characteristics. *Journal of Volcanology and Geothermal Research*, *265*, 78–93.

Hardman, J., Schofield, N., Jolley, D., Hartley, A., Holford, S., & Watson, D. (2019). Controls on the distribution of volcanism and intra-basaltic sediments in the Cambo-Rosebank region, West of Shetland. *Petroleum Geoscience*, *25*(1), 71–89.

Hartley, R. A., Roberts, G. G., White, N., & Richardson, C. (2011). Transient convective uplift of an ancient buried landscape. *Nature Geoscience*, *4*(8), 562–565.

Hayes, S. K., Montgomery, D. R., & Newhall, C. G. (2002). Fluvial sediment transport and deposition following the 1991 eruption of Mount Pinatubo. *Geomorphology*, *45*(3–4), 211–224.

Helland-Hansen, D., Varming, T., & Ziska, H. (2009). Rosebank–challenges to development from a subsurface perspective. In *Faroe Islands Exploration Conference: Proceedings of the 2nd Conference. Annales Societatis Scientarium Faeroensis, Supplementum* (Vol. *50*, pp. 241–245).

Hemelsdaël, R., Ford, M., Malartre, F., & Gawthorpe, R. (2017). Interaction of an antecedent fluvial system with early normal fault growth: Implications for syn-rift stratigraphy, western Corinth rift (Greece). *Sedimentology*, *64*(7), 1957–1997.

Hole, M., Jolley, D., Hartley, A., Leleu, S., John, N., & Ball, M. (2013). Lava–sediment interactions in an Old Red Sandstone basin, NE Scotland. *Journal of the Geological Society*, *170*(4), 641–655.

Hou, G., Qian, X., & Cai, D. (2001). The tectonic evolution of Bohai Basin in Mesozoic and Cenozoic time. *Acta Scientiarum Naturalium-Universitatis Pekinensis*, *37*(6), 845–851.

Houghton, B. F., & Landis, C. A. (1989). Sedimentation and volcanism in a Permian arc-related basin, southern New Zealand. *Bulletin of Volcanology*, *51*(6), 433–450.

Huismans, R., & Beaumont, C. (2011). Depth-dependent extension, two-stage breakup and cratonic underplating at rifted margins. *Nature*, *473*(7345), 74–78.

Huismans, R., & Beaumont, C. (2014). Rifted continental margins: The case for depth-dependent extension. *Earth and Planetary Science Letters*, *407*, 148–162.

Hutchison, W., Pyle, D. M., Mather, T. A., Yirgu, G., Biggs, J., Cohen, B. E., & Lewi, E. (2016). The eruptive history and magmatic evolution of Aluto volcano: New insights into silicic peralkaline volcanism in the Ethiopian rift. *Journal of Volcanology and Geothermal Research*, *328*, 9–33.

Jackson, C. A. L. (2012). Seismic reflection imaging and controls on the preservation of ancient sill-fed magmatic vents. *Journal of the Geological Society*, *169*(5), 503–506.

Jackson, C. A., Schofield, N., & Golenkov, B. (2013). Geometry and controls on the development of igneous sill–related forced folds: A 2-D seismic reflection case study from offshore southern Australia. *Geological Society of America Bulletin*, *125*(11–12), 1874–1890.

Jerram, D. A., Single, R. T., Hobbs, R. W., & Nelson, C. E. (2009). Understanding the offshore flood basalt sequence using onshore volcanic facies analogues: An example from the Faroe-Shetland basin. *Geological Magazine*, *146*(3), 353–367.

Jolley, D. W., Bell, B. R., Williamson, I. T., & Prince, I. (2009). Syn-eruption vegetation dynamics, paleosurfaces and structural controls on lava field vegetation: An example from the Palaeogene Staffa Formation, Mull Lava Field, Scotland. *Review of Palaeobotany and Palynology*, *153*(1–2), 19–33.

Jolley, D. W., Millett, J. M., Schofield, N., & Broadley, L. (2021). Stratigraphy of volcanic rock successions of the North Atlantic rifted margin: The offshore record of the Faroe-Shetland and Rockall basins. *Earth and Environmental Science Transactions of the Royal Society of Edinburgh*, 1–28.

King, B. C., & Chapman, G. R. (1972). A discussion on volcanism and the structure of the earth-volcanism of the Kenya rift valley. *Philosophical Transactions of the Royal Society of London. Series A, Mathematical and Physical Sciences*, *271*(1213), 185–208.

Kirkham, C., Cartwright, J., Hermanrud, C., & Jebsen, C. (2018). The genesis of mud volcano conduits through thick evaporite sequences. *Basin Research*, *30*(2), 217–236.

Leeder, M. R. (2009). *Sedimentology and sedimentary basins: From turbulence to tectonics*. John Wiley & Sons. Multipages.

Leeder, M. R., & Gawthorpe, R. L. (1987). Sedimentary models for extensional tilt-block/half-graben basins. *Geological Society, London, Special Publications*, *28*(1), 139–152.

Leeder, M. R., Mack, G. H., & Salyards, S. L. (1996). Axial–transverse fluvial interactions in half-graben: Plio-Pleistocene Palomas Basin, Southern Rio Grande Rift, New Mexico, USA. *Basin Research*, *8*(3), 225–241.

Li, W., Bhattacharya, J. P., & Campbell, C. (2010). Temporal evolution of fluvial style in a compound incised-valley fill, Ferron "Notom Delta", Henry Mountains region, Utah (USA). *Journal of Sedimentary Research*, *80*(6), 529–549.

Liu, Q. H. (2016). *"Source-to-Sink" system coupling analysis of the Palaeogene, Shaleitian uplift, Bohai Bay Basin, China (Doctoral thesis)*. China University of Petroleum (Beijing).

Liu, Q. H., Zhu, X. M., Li, S. L., Xu, C. G., Du, X. F., Li, H. Y., & Shi, W. L. (2017). Source-to-sink system of the steep slope fault in the western Shaleitian uplift. *Earth Science*, *42*(11), 1883–1896.

Lu, K. Z., & Dai, J. S. (1989). Structural characteristics and evolution of upper proterozoic in central Hebei rift valley. *Journal of China University of Petroleum*, *2*, 6–17.

Lunt, I. A., Bridge, J. S., & Tye, R. S. (2004). A quantitative, three-dimensional depositional model of gravelly braided rivers. *Sedimentology*, *51*(3), 377–414.

Magee, C., Bastow, I. D., van Wyk de Vries, B., Jackson, C. A. L., Hetherington, R., Hagos, M., & Hoggett, M. (2017). Structure and dynamics of surface uplift induced by incremental sill emplacement. *Geology*, *45*(5), 431–434.

Magee, C., Jackson, C. A. L., & Schofield, N. (2013). The influence of normal fault geometry on igneous sill emplacement and morphology. *Geology*, *41*(4), 407–410.

Magee, C., Jackson, C. L., & Schofield, N. (2014a). Diachronous sub-volcanic intrusion along deep-water margins: Insights from the Irish Rockall Basin. *Basin Research*, *26*(1), 85–105.

Magee, C., McDermott, K. G., Stevenson, C. T., & Jackson, C. A. L. (2014b). Influence of crystallised igneous intrusions on fault nucleation and reactivation during continental extension. *Journal of Structural Geology*, *62*, 183–193.

Magee, C., Muirhead, J. D., Karvelas, A., Holford, S. P., Jackson, C. A., Bastow, I. D., & Shtukert, O. (2016). Lateral magma flow in mafic sill complexes. *Geosphere*, *12*(3), 809–841.

Manville, V., Hodgson, K. A., & Nairn, I. A. (2007). A review of break-out floods from volcanogenic lakes in New Zealand. *New Zealand Journal of Geology and Geophysics*, *50*(2), 131–150.

Manville, V., Németh, K., & Kano, K. (2009). Source to sink: A review of three decades of progress in the understanding of volcaniclastic processes, deposits, and hazards. *Sedimentary Geology*, *220*(3–4), 136–161.

Martí, J., Groppelli, G., & da Silveira, A. B. (2018). Volcanic stratigraphy: A review. *Journal of Volcanology and Geothermal Research*, *357*, 68–91.

Menzies, M. A., Klemperer, S. L., Ebinger, C. J., & Baker, J. (2002). Characteristics of volcanic rifted margins. *Special Papers-Geological Society of America*, 1–14.

Miles, A., & Cartwright, J. (2010). Hybrid flow sills: A new mode of igneous sheet intrusion. *Geology*, *38*(4), 343–346.

Millett, J. M., Hole, M. J., Jolley, D. W., Passey, S. R., & Rossetti, L. (2020). Transient mantle cooling linked to regional volcanic shut-down and early rifting in the North Atlantic Igneous Province. *Bulletin of Volcanology*, *82*(8), 1–27.

Millett, J. M., Hole, M. J., Jolley, D. W., Schofield, N., & Campbell, E. (2016). Frontier exploration and the North Atlantic Igneous Province: New insights from a 2.6 km offshore volcanic sequence in the NE Faroe-Shetland Basin. *Journal of the Geological Society*, *173*(2), 320–336.

Millett, J. M., Jerram, D. A., Manton, B., Planke, S., Ablard, P., Wallis, D., & Dennehy, C. (2021). The Rosebank Field, NE Atlantic: Volcanic characterisation of an inter-lava hydrocarbon discovery. *Basin Research*.

Miyabuchi, Y. (1999). Deposits associated with the 1990–1995 eruption of Unzen volcano, Japan. *Journal of Volcanology and Geothermal Research*, *89*(1–4), 139–158.

Muirhead, J. D., Van Eaton, A. R., Re, G., White, J. D., & Ort, M. H. (2016). Monogenetic volcanoes fed by interconnected dikes and sills in the Hopi Buttes volcanic field, Navajo Nation, USA. *Bulletin of Volcanology*, *78*(2), 11.

Muravchik, M., D'Elia, L., Bilmes, A., & Franzese, J. R. (2011). Syn-eruptive/inter-eruptive relations in the syn-rift deposits of the Precuyano Cycle, Sierra de Chacaico, Neuquén Basin. *Argentina. Sedimentary Geology*, *238*(1–2), 132–144.

Planke, S. (1994). Geophysical response of flood basalts from analysis of wire line logs: Ocean drilling program site 642, Vøring volcanic margin. *Journal of Geophysical Research: Solid Earth*, *99*(B5), 9279–9296.

Planke, S., Millett, J. M., Maharjan, D., Jerram, D. A., Abdelmalak, M. M., Groth, A., & Myklebust, R. (2017). Igneous seismic geomorphology of buried lava fields and coastal escarpments on the Vøring volcanic rifted margin. *Interpretation*, *5*(3), SK161–SK177.

Planke, S., Rasmussen, T., Rey, S. S., & Myklebust, R. (2005). Seismic characteristics and distribution of volcanic intrusions and hydrothermal vent complexes in the Vøring and Møre basins. In *Geological Society, London, Petroleum Geology Conference series* (Vol. *6*, No. 1, pp. 833–844). Geological Society of London.

Planke, S., Symonds, P. A., Alvestad, E., & Skogseid, J. (2000). Seismic volcanostratigraphy of large-volume basaltic extrusive complexes on rifted margins. *Journal of Geophysical Research: Solid Earth*, *105*(B8), 19335–19351.

Prather, B. E., Booth, J. R., Steffens, G. S., & Craig, P. A. (1998). Classification, lithologic calibration, and stratigraphic succession of seismic facies of intraslope basins, deep-water Gulf of Mexico. *AAPG Bulletin*, *82*(5), 701–728.

Ravnås, R., & Steel, R. J. (1998). Architecture of marine rift-basin successions. *AAPG Bulletin*, *82*(1), 110–146.

Reynolds, P., Schofield, N., Brown, R. J., & Holford, S. P. (2018). The architecture of submarine monogenetic volcanoes–insights from 3D seismic data. *Basin Research*, *30*, 437–451.

Riggs, N. R., Hurlbert, J. C., Schroeder, T. J., & Ward, S. A. (1997). The interaction of volcanism and sedimentation in the proximal areas of a mid-Tertiary volcanic dome field, central Arizona, USA. *Journal of Sedimentary Research*, *67*(1), 142–153.

Schofield, N., Holford, S., Millett, J., Brown, D., Jolley, D., Passey, S. R., & Stevenson, C. (2017). Regional magma plumbing and emplacement mechanisms of the Faroe-Shetland Sill Complex: Implications for magma transport and petroleum systems within sedimentary basins. *Basin Research*, *29*(1), 41–63.

Schofield, N., & Jolley, D. W. (2013). Development of intra-basaltic lava-field drainage systems within the Faroe-Shetland Basin. *Petroleum Geoscience*, *19*(3), 273–288.

Schofield, N., Newton, R., Thackrey, S., Watson, D., Jolley, D., & Morley, C. (2021). Linking surface and subsurface volcanic stratigraphy in the Turkana depression of the East African Rift system. *Journal of the Geological Society*, *178*(1).

Shi, W., Zhang, Z., Peng, W., & Tao, G. (2013). Tectonic evolution and hydrocarbon accumulation in the east part of Shaleitian Aailent, Western Bohai Sea. *Oil & Gas Geology*, *34*(2), 242–247.

Sulpizio, R., Mele, D., Dellino, P., & La Volpe, L. (2007). Deposits and physical properties of pyroclastic density currents during complex Subplinian eruptions: The AD 472 (Pollena) eruption of Somma-Vesuvius, Italy. *Sedimentology*, *54*(3), 607–635.

Svensen, H., Jamtveit, B., Planke, S., & Chevallier, L. (2006). Structure and evolution of hydrothermal vent complexes in the Karoo Basin, South Africa. *Journal of the Geological Society*, *163*(4), 671–682.

Thomson, K. (2005). Volcanic features of the North Rockall Trough: Application of visualisation techniques on 3D seismic reflection data. *Bulletin of Volcanology*, *67*(2), 116–128.

Umazano, A. M., Melchor, R. N., Bedatou, E., Bellosi, E. S., & Krause, J. M. (2014). Fluvial response to sudden input of pyroclastic sediments during the 2008–2009 eruption of the Chaitén Volcano (Chile): The role of logjams. *Journal of South American Earth Sciences*, *54*, 140–157.

Vessell, R. K., & Davies, D. K. (1981). Nonmarine sedimentation in an active fore arc basin.

Walker, F., Schofield, N., Millett, J., Jolley, D., Holford, S., Planke, S., & Myklebust, R. (2021). Inside the volcano: Three-dimensional magmatic architecture of a buried shield volcano. *Geology*, *49*(3), 243–247.

White, R., & McKenzie, D. (1989). Magmatism at rift zones: The generation of volcanic continental margins and flood basalts. *Journal of Geophysical Research: Solid Earth*, *94*(B6), 7685–7729.

Williamson, I. T., & Bell, B. R. (2012). The staffa lava formation: Graben-related volcanism, associated sedimentation and landscape character during the early development of the Palaeogene Mull Lava Field, NW Scotland. *Scottish Journal of Geology*, *48*(1), 1–46.

Wolfenden, E., Ebinger, C., Yirgu, G., Renne, P. R., & Kelley, S. P. (2005). Evolution of a volcanic rifted margin: Southern red

sea, Ethiopia. *Geological Society of America Bulletin*, *117*(7–8), 846–864.

Xu, C. G., Yu, S., Lin, C. S., Wang, X., Wang, Y. C., & Li, H. Y. (2008). Structural styles of the Palaeogene lacustrine basin margin and their control on sedimentary sequences in Bohai Sea area. *Journal of Palaeogeography*, *10*(6), 627–635.

Zanchetta, G., Sulpizio, R., & Di Vito, M. A. (2004). The role of volcanic activity and climate in alluvial fan growth at volcanic areas: An example from southern Campania (Italy). *Sedimentary Geology*, *168*(3–4), 249–280.

Zhang, G. C. (2000). Tectonic framework and distribution of hydrocarbon-rich depressions in the Bohai Sea. *China Offshore Oil and Gas (Geology)*, *14*(2), 93–99.

Zhu, W. L., Wu, J. F., & Zhang, G. C. (2015). Tectonic differential evolution of the Cenozoic basins in the offshore China and the direction of oil and gas exploration. *Geoscience Frontier*, *22*(1), 88–101.

Zou, C. N., Zhao, W. Z., Jia, C. Z., Zhu, R. K., Zhang, G. Y., Xia, Z., & Yan, X. J. (2008). Formation and distribution of volcanic hydrocarbon reservoirs in sedimentary basins of China. *Petroleum Exploration and Development*, *35*(3), 257–271.

How to cite this article: Chen, H., Zhu, X., Gawthorpe, R. L., Wood, L. J., Liu, Q., Li, S., Shi, R., & Li, H. (2022). The interactions of volcanism and clastic sedimentation in rift basins: Insights from the Palaeogene-Neogene Shaleitian uplift and surrounding sub-basins, Bohai Bay Basin, China. *Basin Research*, 00, 1–28. https://doi.org/10.1111/bre.12651